December 2017/January 2018
Volume 124
Issue 1978
£5.90

www.electronicsworld.co.uk

Electronics WORLD

THE ESSENTIAL ELECTRONICS ENGINEERING MAGAZINE

SPECIAL REPORT
ANALOGUE DESIGN:
- Linear change of voltages and generating complementary voltages
- Chaotic and complex non-linear circuits

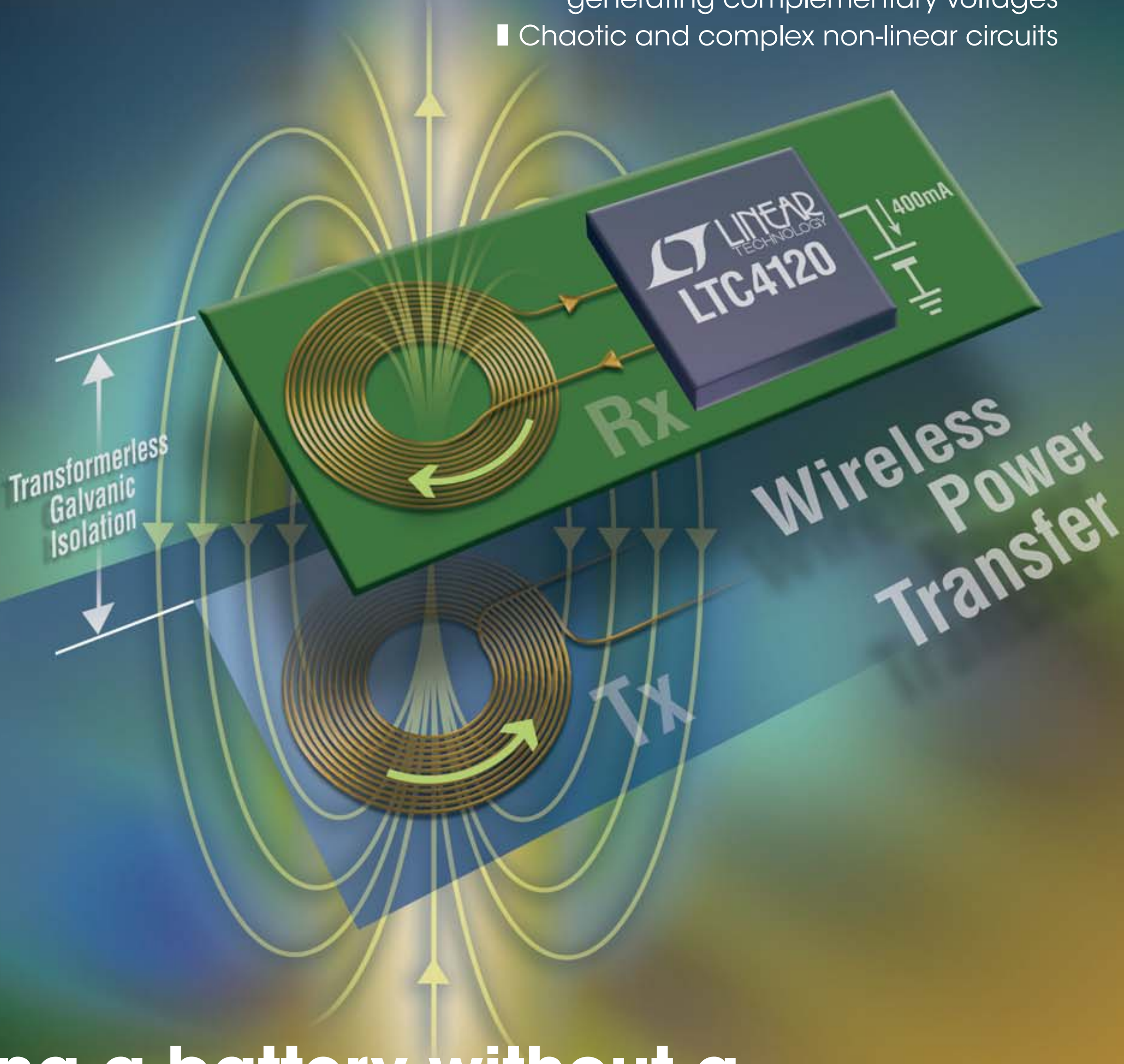

Charging a battery without a connector – made easy

by Linear Technology, now part of Analog Devices

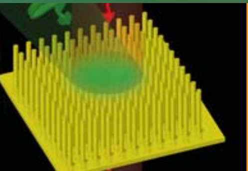

Trend
New, ultra-fast method of changing fundamental property of light

CMOS Clocks
CMOS vs LVCMOS: Which is the best for your application?

Latest Products
German Industry 4.0 expertise goes to China

Cover supplied by LINEAR TECHNOLOGY, now part of Analog Devices
More on pages 6-7

REGULARS

FEATURES

TEST & MEASUREMENT SUPPLEMENT

IS YOUR DISHWASHER SAFE FROM HACKERS?

There was a security alert issued earlier this year for, of all things, a dishwasher! The Miele Professional PG 8528 PST10 is a commercial machine that contained a severe ‘directory traversal’ vulnerability that could ultimately allow hackers to exploit and interfere with its normal operation. For those who don’t know, directory traversal is an HTTP exploit that allows attackers to access restricted directories and execute commands outside the web server’s root directory.

Of even greater concern was that there was no known patch for the vulnerability, exposing a fear of many security professionals that, in their bid to be first to market with new products, traditional device manufacturers are ill-equipped to manage the security aspect of smart, connected devices, treating security as an afterthought.

The rise of the Internet of Things (IoT) is forcing manufacturers to move out of their comfort zones and into areas away from their primary skills, including software development and security.

As they start connecting more of their products to the Internet, focus on security during development is a must. This includes careful code testing, continuing maintenance, careful mapping of bundled software, and verified intelligence about software vulnerabilities in that software, as well as ample resources to react promptly and effectively as soon as a vulnerability in the product is reported.

Fortunately, new technologies are now available so application producers can provide customers with updates, reducing risk exposure and potential liability. However, this still requires manufacturers to have a software vulnerability management strategy, because if a product is connected to the Internet, it can probably be hacked.

Top Priority

Security measures should be applied at all layers of the device’s firmware and software. It is important that these processes be stable and work in the greater IoT ecosystem, where software is part of the longer supply chain, or might be bundled with applications from other vendors.

Open Source Software (OSS) is used extensively by virtually all software developers and is part of almost every IoT solution. Despite its ubiquity, OSS is largely unmanaged, which means that developers are unable to track and mitigate vulnerabilities in their code. Continuous analysis of the source code will enable them to keep all OSS and third-party components up to date, and react when a vulnerability occurs.

“Despite its ubiquity, OSS is largely unmanaged, which means that developers are unable to track and mitigate vulnerabilities in their code

Once software gets distributed, applications should be tamper-resistant so they become very hard for hackers to get access to the code. In addition, secure and mature licensing technologies should be applied to ensure that only eligible users can access the applications.

Stable and scaleable update processes and technologies should be in place from day one so that producers can update software or firmware on devices in the field, in case a software vulnerability has been detected and needs to be patched, or in case of a hack, which – unfortunately – can happen.

Tips For The IoT

IoT producers should follow the following three tips to ensure application security in an IoT world:

1. Scan codebase for OSS and third-party components that might be riddled with vulnerabilities.
2. Protect apps against hacking with tamper-resistant licensing and applications.
3. Be prepared with an automated and continuous software/firmware update solution and react quickly when a software vulnerability needs patching or a hack occurs.

It goes without saying that IoT devices are getting smarter as technology advances. As we have seen time and time again, innovation always comes with inherent risks. Manufacturers and organisations continue to share the burden of taking the necessary precautions to help ensure their devices are not easy prey for criminals.

By Steve Dunnigan, Regional Vice President, Flexera Software (www.flexera.com)

EDITOR:
Svetlana Josifovska
Tel: +44 (0)1732 883392
Email: svetlanaj@sjpbusinessmedia.com

SALES:
Suzie Pipe
Tel: +44 (0)20 8306 0564 | Mobile: +44 (0)7799 063311
Email: suziep@electronicsworld.co.uk

DESIGN: Tania King

PUBLISHER: Wayne Darroch

ISSN: 1365-4675

PRINTER: Buxton Press Ltd

SJP business media
2nd Floor,
52-54 Gracechurch Street,
London, EC3V 0EH

SUBSCRIPTIONS:
Subscription rates:
UK - 1 year digital only £53.00+VAT
UK - 1 year print and digital sub £68.00
UK - 2 year print and digital sub £109.00
UK - 3 year print and digital sub £143.00
International - 1 year digital only £53.00
International - 1 year print and digital sub £164.00
International - 2 year print and digital sub £290.00
International - 3 year print and digital sub £409.00
Tel/Fax +44 (0)1635 879361/868594
Email: electronicsworld@circdata.com
www.electronicsworld.co.uk/subscribe

Follow us on Twitter @electrowo

Join us on LinkedIn

DEKRA BUILDS TEST AREA FOR CONNECTED DRIVING IN MALAGA

Automotive solutions supplier Dekra is building a connected-car test area in Malaga, Spain, as part of an international testing network for automated driving.

The setup joins Dekra's other facilities in Klettwitz and Lausitzring in Germany, to focus on R&D and early production testing, which will also include infrastructure testing. Dekra plans to add more hubs in East Asia and the US, while simultaneously developing test setups and tools, and fostering standardisation in the industry. The network is expected to help partners start future-proofing their automotive solutions.

"We have developed a significant number of test scenarios, some of which have already been implemented. They verify the generation and reception of appropriate signalling messages and corresponding warnings to drivers," said Fernando Hardasmal, Managing Director of Dekra Testing & Certification. "Some of the scenarios tested for vehicle-to-everything technologies, also referred to as V2X, are Intersection Movement Assist, Green Light Optimal Speed Advisory, Forward Collision Warning and Work Zone Warnings".

In addition to deploying actual V2X devices, Dekra will use dedicated beacons and purpose-built software. Activities in this area will focus on interoperability, performance and usability testing, as well as cyber-security evaluations for the connected car.

The new 50,000m² test area is being built in the Andalusia Technology Park in Malaga, to open at the end of 2017.

SCIENTISTS DEVELOP AN ULTRA-FAST METHOD OF CHANGING FUNDAMENTAL PROPERTY OF LIGHT

Scientists at King's College London have developed a new way to rapidly change the polarisation of light, one of its fundamental properties, leading to much faster data transfer and advanced development of nano-materials.

Polarised light waves are those in which the electric and magnetic vibrations occur in a single plane. The polarisation of light is changed by the material it passes through, so it can be used to learn about nano-scale processes, such as quantum electronics. Polarisation switching is also used to transfer digital information in fibre optic cables.

The electronic methods used to control light polarisation are reaching their physical speed limit, but researchers at King's have overcome this, allowing polarisation to be switched hundreds of times faster.

To do this they designed nano-structured materials that control polarisation using light itself – a technique known as 'all-optical polarisation control'. These nano-structures are known as metamaterials: materials with optical properties not available in nature. These thin, lightweight materials are made from elements smaller than a thousandth of a millimetre to create optical effects. In this case, the metamaterial consists of gold nano-particles.

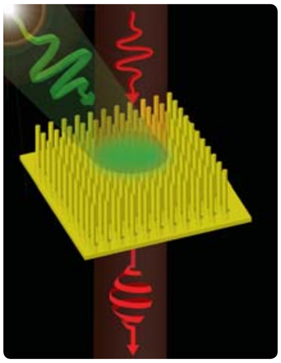

High-intensity light pulse is fired onto a metamaterial to change its refractive index

CONNECTIVITY CONCERNS MUST BE ADDRESSED TO UNLOCK IOT'S POTENTIAL FOR THE ENERGY SECTOR

Energy companies will struggle to derive the maximum value from the Internet of Things (IoT) without access to radically-improved, reliable, high-speed connectivity. So states independent research commissioned by the satellite network operator Inmarsat, which found that, while most energy companies are in the process of introducing or developing IoT solutions, low rates of connectivity are preventing them from realising the full benefits.

Respondents from 100 large energy companies worldwide were interviewed for Inmarsat's '*The Future of IoT in Enterprise – 2017*' report, which found that lack of connectivity emerged as the top obstacle energy companies face when introducing IoT. Some 54% of the respondents cited connectivity as a major challenge, significantly higher than the percentage citing skills and cyber security as challenges (35% and 27%, respectively). Lack of high-speed connectivity may keep these companies from accessing the full value offered by IoT, potentially rendering them unable to gather and analyse data.

Worryingly, 24% of respondents agreed that connectivity issues threaten to derail their IoT projects before they even begin, further emphasising the connectivity problems facing the sector.

Commenting on the significance of the findings, Chuck Moseley, Senior Director for Energy at Inmarsat Enterprise, said: "Connected sensors can gather vital data in a wide range of applications, offering energy companies an unprecedented opportunity to improve safety, improve operating efficiencies and reduce production costs. For example, oil producers and pipeline operators can use sensors to monitor hundreds of wells in real time, to understand the amount and quality of the oil and gas being extracted or moved. They can also monitor for downtime, unusual behaviour or even accidental leaks, putting them in a stronger position to take pre-emptive action. Energy companies who want to use IoT in this way need to have a constant, uninterrupted stream of data to make informed decisions about their operations, but to achieve that you need access to a robust, reliable communications network."

CHARGING A BATTERY WITHOUT A CONNECTOR – MADE EASY

By Tony Armstrong, Director of Product Marketing for Power Products at Linear Technology, now part of Analog Devices

Lots of products use a battery as the primary power source. Of course, we all know about the "i-something" products with the fruit logo on them. However, there are plenty of less glamorous products that serve equally deserving applications that also use batteries. I am talking about portable medical devices, industrial sensors and even rotating or moving equipment. Unlike the benign consumer environment, these applications have more stringent requirements such as the need for sterilisation and even the potentially explosive surroundings like those commonly found in oil refineries and chemical processing facilities.

In many of these applications, a connector for charging purposes is difficult or impossible to use. For example, some products require sealed enclosures to protect sensitive electronics from harsh environments. Others may simply be too small to include a connector. And in products where the battery-powered application includes movement or rotation, it is virtually impossible to have charging with wires.

Therefore, what alternative method can be employed to deal with these circumstances? Well, it is clearly one that eliminates the connector and would be wireless charging capable. A wireless charging solution adds value, reliability and robustness in these applications where connectors cannot.

Wireless Power Transmission

So if wireless charging is a good solution in those instances where a connector cannot be used, what is it and how is it accomplished? Well, a simple and straightforward definition might be: wireless power is the transmission of electrical energy from a power source to an electrical load without the use of man-made conductors.

However, this tends to be a little too simplistic to demonstrate the challenges involved in performing this process. Therefore, I wish to provide you with a more in-depth explanation before we move onto the constraints and methods to overcome them are discussed. So, let's start with the basics: an electric current flowing through a conductor, such as a wire, carries electrical energy. When an electric current passes through a circuit (or wire) there is a magnetic field in the area surrounding the conductor.

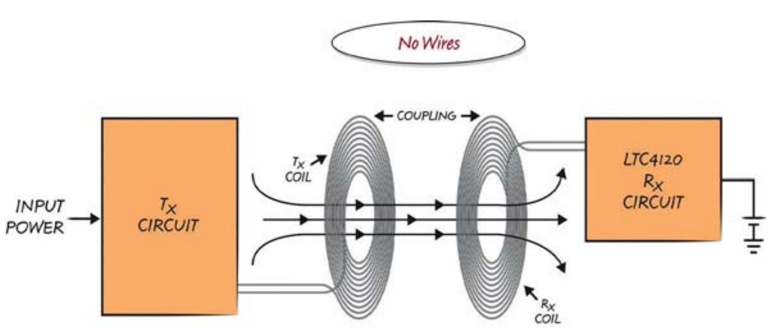

Figure 1: Wireless power transfer from a primary transmit coil (Tx) to a secondary receive coil (Rx), including the LTC4120

In a circuit with alternating current, there exists a time-varying magnetic field in the vicinity of the wire. And if a conductor is placed into this time-varying field, a current is induced.

One common occurrence in electronic systems is electrical transients such as lightning strikes from an external source or capacitor discharge, which could be an internal repetitive disturbance such as in the condenser discharge of an ignition system.

The magnetic field intensity is proportional to the magnitude of the current flowing in the conductor. Energy is transferred from a conductor that produces the fields (the primary) to any conductor on which the fields impinge (the secondary) via the magnetic coupling defined above. In a loosely coupled system where the coupling coefficient is low, a high frequency current does not pass for long distances along a conductor but rapidly loses energy because of the impedance mismatch along the cable, which causes the energy to be reflected back to the source or radiated into the air. See the illustration in Figure 1 for a graphical representation of loosely coupled windings connected via a magnetic field. It should be noted that this figure also shows the LTC4120, which will be discussed in more detail later in this article.

Battery Charging from Wireless Power

When designing a wireless power charging system, a key parameter is the amount of charging power that actually adds energy to the battery. This received power depends on many factors, including the amount of power being transmitted, the distance and alignment between the transmit coil and the receive coil also known as the coupling between the coils, and finally the tolerance of the transmit and receive components.

The primary goal in any wireless power design is to guarantee delivery of the required power under worst-case power transfer conditions. However, it is equally important to avoid thermal and electrical overstress in the receiver during best-case conditions. This is especially important when output power requirements are low. Take for example when the battery is fully charged or nearly fully charged and the coils are in close proximity to each other. In such a scenario, available power from the wireless system is high, but demanded power is low. This excess power typically leads to high rectified voltages or a need to dissipate the excess power as heat.

There are several ways to deal with excess power capacity when the demanded receiver power is low. The rectified voltage can be clamped with a power Zener diode or transient voltage suppressor. However, this solution is typically large and generates considerable heat. The transmitter power can be reduced, but this will either limit the available received power or it will reduce the transmit distance. It is also possible to communicate received power back to the transmitter and adjust transmit power accordingly. This is the technique used by wireless power standards such as the Wireless Power Consortium Qi standard. However, it is also possible to solve this issue in a compact and efficient manner without resorting to complicated digital communication techniques. Techniques that communicate via small variations in the transmitted power level require a minimum amount of power transmission and may not work for systems with variable transmit distances.

An Easy To Use IC for Wireless Charging

To meet these goals, Linear Technology's LTC4120 wireless power receiver and battery charger integrates technology by PowerbyProxi, Linear Technology's technology partner. PowerbyProxi's patented Dynamic Harmonisation Control (DHC), technique enables high efficiency contactless charging without thermal or electrical overstress concerns in the receiver. Using this technology, up to 2W can be transmitted at a distance of up to 1.2cm. However, for single-cell Li-Ion batteries, the maximum charge voltage of 4.2V and maximum charge current of 400mA will limit this value to 1.7W. Similarly, the 2W maximum will limit 2 Series Li-Ion batteries (8.4V maximum charge voltage) to 240mA of charge current.

The metrics of power, efficiency, range and size determine system performance and so the LTC4120-based wireless power system was designed to receive up to 2W at the battery up to a distance of 1.2cm when used with one of several transmitter options. Efficiency calculations vary tremendously based on the technique and components used. Typically, the battery will receive 45% – 55% of the DC input power fed to the transmitter in an LTC4120-based system.

PowerbyProxi's DHC tuning technology embedded in the LTC4120 provides significant advantages over other wireless power solutions. In response to environmental and load changes, DHC dynamically varies the resonant frequency of the resonant tank circuit on the receiver. DHC achieves greater power transfer efficiency, enabling smaller receiver sizes, even as it allows greater transmission range. Unlike other wireless power transfer technologies, DHC enables intrinsic power level management as part of the inductive power field, eliminating the need for a separate communication channel to validate receivers or to manage variation in load demand during the battery charge cycle.

It is clear that DHC solves a problem fundamental to all wireless power systems. Every system must be designed to receive a certain amount of power at a given maximum transmit distance. Every system must also be designed to survive a no-load condition at minimum transmit distance. The competitive alternatives solve this problem with a complicated digital communication system that adds complexity and cost, limiting power transmission distance. The LTC4120-based

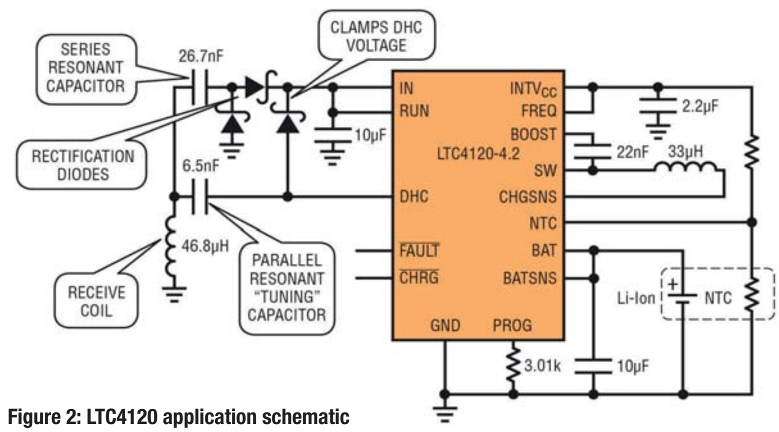

Figure 2: LTC4120 application schematic illustrates a complete wireless battery charging circuit

wireless power system easily solves this problem by incorporating PowerbyProxi's DHC technology.

The Linear Technology and PowerbyProxi Relationship

PowerbyProxi has been working to deliver wireless power solutions for industrial customers since 2007. Rather than invest a great deal of money into its own marketing efforts, they decided to develop and improve their technology and to partner with industry leaders such as Linear Technology to bring the technology to market. With significant success and a broad portfolio of technology embodiments to its credit, they are now gaining recognition as the leading global wireless power company.

One of the key reasons why Linear Technology partnered with PowerbyProxi was due to their significant IP portfolio and solution design know-how that offers customers the leading technology in the industry and also assurance that the technology is fully backed by IP. PowerbyProxi has more than 30 patents in process and many more in the review and filing stages, making them the leading innovator and IP leader in the wireless power field.

Conclusion

Outside of the mass consumer market for the wireless charging of "i" this, or "robot" that, there is a class of portable industrial and medical products where the ability to wirelessly charge their internal batteries across air gaps or through non-ferrite materials up to a centimeter or so, is a "must have" requirement for their deployment. Up until now, a design engineers' options have had limitations, which have hindered their end products' success and viability. Fortunately, thanks to the recent introduction of the LTC4120 from Linear Technology, that's all about to change. This highly integrated IC, which can wirelessly receive power transmitted from a coil of up to 1.2cm apart, as well as charge a battery, provides a simple and effective solution. It is the embodiment of wireless charging made easy – no connectors necessary!

Linear Technology (UK) Ltd, now part of Analog Devices
• Tel: 01628 477066 • Email: uksales@linear.com
• www.linear.com

App-dates

BY **LUCIO DI JASIO**, MCU8 BUSINESS DEVELOPMENT MANAGER AT MICROCHIP TECHNOLOGY

This morning, as soon as I turned on my (smart) phone I had a notification: 18 applications were imploring me to update them. Again?! I'm sure I updated most of them only last week! What does this say about their developers' abilities if they need so many fixes on a weekly basis?

Of course, this has been happening a lot recently, and it's clear that there is some true bug-fixing going on, but there must also be some other perverse mechanism at play that encourages developers to re-spin their apps at such a dizzying pace. Imagine if we were to update all our embedded applications with the same frequency?

On the other hand, I do remember the days when One Time Programmable (OTP) devices were the norm and, before that, there was a time when microcontrollers could only be manufactured with immutable ROM code.

Figure 1: My App-dates awaiting

That was risky business! Any small bug could turn into a significant monetary loss since even the smallest production runs could mean (tens of) thousands of devices had to be scrapped and a new 'mask' launched.

OTP changed all that in the 90s, when EPROMs replaced the microcontrollers' ROMs. In the beginning OTP was limited to very small quantities, since the devices had tiny, expensive, quartz 'windows' on ceramic packages. The windows were used to erase the EPROM contents using ultra-violet lamps.

Microchip championed that technology and made all PIC microcontrollers exclusively in OTP technology from day one. The expensive windows were still available, but only on development units. Production devices could fit into much cheaper, windowless, plastic packages. Design risk was significantly minimised, since the technology allowed 'on-demand' or 'just-in-time' programming of the minimum (daily) quantities required.

Next, electrically-erasable programmable read-only memory (EEPROM) became available and turned into what today we refer to as Flash. Microchip once more jumped with both feet into the novel technology – in 1995 the first EEPROM-based PIC16C84 was born – and by the new millennium all new PIC microcontrollers were designed exclusively with Flash. (Incidentally, the 'C84 was renamed 'F84 only a couple of years later, since the term 'Flash' had become such a strong industry buzzword).

Flash-Programming, Re-Programming, Self-Programming

In the beginning, the main perceived advantage of Flash technology was its ability to inexpensively program a microcontroller more than once. With Flash, as soon as a bug was discovered, developers could immediately work on a fix and proceed to re-program any batch of devices that had not been mounted or shipped.

As soon as In-Circuit-Serial-Programming (ICSP) techniques were introduced, this meant that even if already mounted on a board, shipped (and returned) products could be fixed/upgraded as needed, by connecting the appropriate programmer/debugger tool.

Even better, if the Flash microcontrollers had a capable internal charge pump – the physics of Flash technology requires high voltage (typically ~22V) to be applied to a memory cell for programming and erasing – self-programming became possible. An application/product could now receive updates via any number of communication interfaces and apply them to the device's own program memory.

This might sound like such an obvious feature now, but the reality is that, for all the talking about the benefits of Flash infinite re-programmability, embedded applications that took advantage of this feature were few and far between.

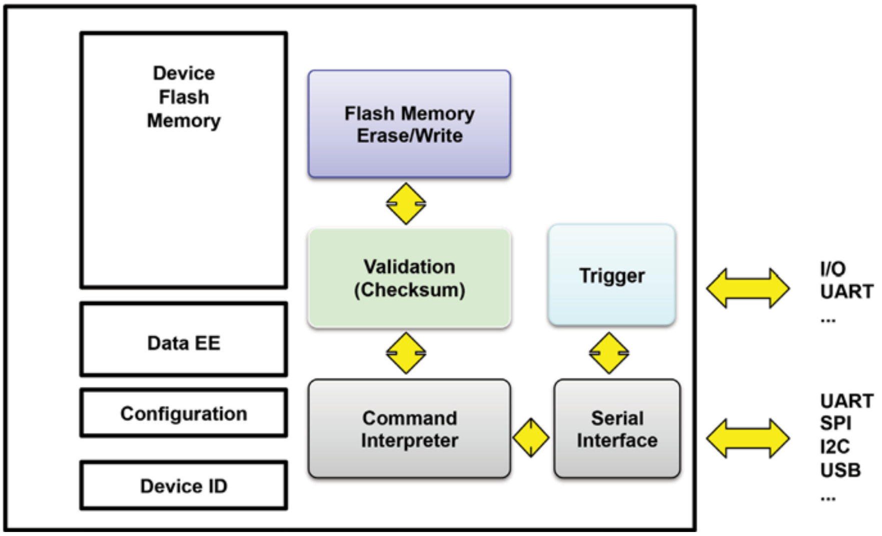

Figure 2: Block diagram of a bootloader

Getting The Boot (-Loader)

I daresay that most of the actual in-circuit re-programming of Flash microcontrollers in the past decade was relegated to the realm of development boards and tools.

This appears to have changed in the last few years. The explosion in connectivity technologies at the root of the IoT frenzy means that today it is easier than ever to connect to a microcontroller in the field, and there is more motivation to update/fix its code as the pace of innovation accelerates.

Enter the bootloader, a (hopefully) small application that sits mostly in the background and is occasionally used to bootstrap, self-program and launch the actual product application – you must have certainly encountered one if you've ever used an Arduino, MikroMedia or Clicker board.

> "As soon as ICSP techniques were introduced, this meant that even if already mounted on a board, shipped (and returned) products could be fixed/upgraded as required, by connecting the appropriate programmer/debugger tool

In fact, bootloaders come in many shapes and forms – as diverse as the microcontroller and its applications. While there is no 'perfect' bootloader for all purposes, you won't find anything close to a standard out there. There are many common features and challenges that every embedded bootloader design must encompass, including:

- A trigger, which is an input, event or condition that's meant to force the device to launch the bootloader code rather than the default application. This can be as simple as a pushbutton or a switch detecting new media being inserted into a slot, or a check that is performed on the first few bytes received at powerup within the first few seconds.
- A visual indicator, used to signal when the bootloader is active and awaiting data/code. This can be a simple LED.
- An agreed communication channel, typically represented by one or more serial communication ports (UART, SPI, I2C, USB, Ethernet…).
- A small and well-documented set of commands to be used over the above communication channel(s). Most bootloaders use simple single-byte codes to identify a small set of commands.
- A validation mechanism, to verify the integrity of the data/code received. This can be as simple as a checksum, or a CRC.
- Optionally, encryption/authentication mechanisms can be added to ensure the data/code can be transported securely, and to prevent hackers from compromising the product.

For most bootloaders there's also a counterpart PC application used to perform the upload. This can be omitted when a more sophisticated bootloader can directly access a mass-storage device (such as an SD card or a USB Flash stick) carrying a file with a convened signature/name.

Linking Loaders

At this point you might wonder if bootloaders are not to also be found on personal computers and smartphones. This is true but since most/all modern operating systems use a Memory Management Unit (MMU) and implement a virtual memory space, in those cases we refer to "linking loaders". This is a very complex category of its own that we won't cover here just now. Instead, I will focus on simple microcontroller applications developed on bare metal or, at best, in conjunction with an embedded RTOS that will be considered an integral part of the application.

Going High Or Low

Before we start writing a bootloader of our own, there is one last fundamental decision to make: to go high or low.

Granted, the bootloader will occupy a (hopefully) very small amount of Flash memory; we'll need to decide where to put it so it doesn't overlap with the user applications.

If we go low (as in Figure 2), we will overlap the reset and interrupt vector(s) table. Hence the need to forward them to addresses higher in the memory space, past the bootloader's >

Figure 3: Low-side bootloader

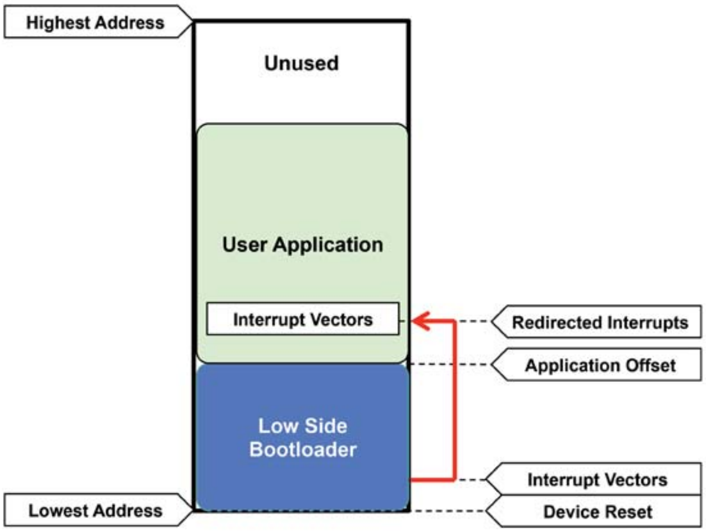

own code. But since the entire application code will have to move "up" as well, low-side bootloaders force each application to be re-compiled (linked) to ensure compatibility with the new vector- and code locations. Depending on the chosen microcontroller and toolchain, this can be as simple as providing an offset in the project properties (see Figure 3 for an MPLAB XC8 compiler example), or by manually editing a linker script (see Listing 1 for a snippet from an MPLAB XC32 compiler example).

If we place the bootloader at the highest range of available memory space (Figure 4), we won't be overlapping the interrupt vector(s) and, if the user applications are not going to use up all the Flash memory, there is no need to modify them at all. That means no linker scripts and no special project configurations are needed. There is a little extra work necessary only on the bootloader side (or on the application/GUI that connects to it) to intercept the reset vector. This can be done entirely automatically, though, by modifying the reset vector to point to the bootloader first (Listing 2).

The popular MikroElektronika series of MikroMedia and Clicker development boards uses a high-side bootloader. For a sample implementation (in Python) of their PC GUI, see link [3] in the box on the last page of this feature.

On the other hand, Arduino and most small microcontroller bootloaders are of the low-side type.

Bootloaders need to be small relative to the size of available Flash memory, but this doesn't mean they are difficult to write, or need to be in assembly language. On the contrary, it is possible to write very compact bootloaders in C, especially if the communication interface is a simple UART, SPI or I2C port. See links [9] and [10] for examples of a minimal PIC I2C bootloader and a UART PIC bootloader. >

Figure 4: MPLAB XC8 configuration

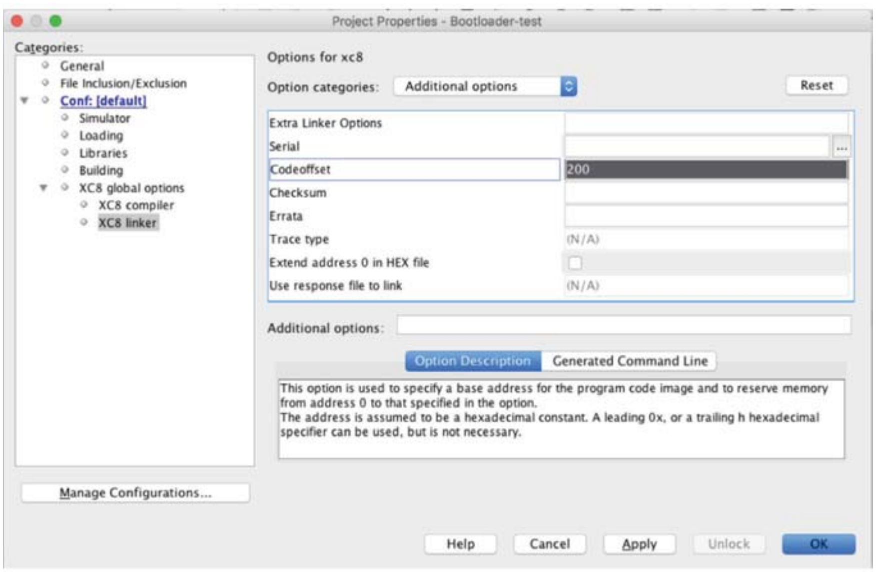

300 Watts AC-DC Power Supply
Industry Standard 3 x 5 inch
Open PCB Single Outputs

NEW

PSY300 Series

Features

- Compact 3 x 5” footprint
- 90-264VAC input with active Power Factor Correction
- 200W convection cooled 300W with forced air cooling
- Wide operating temperature range of -30° to +85°C with derating
- High efficiency up to 92%
- Built in remote sense and power fail signal
- Short circuit, over current, over voltage and over temp. protection
- 12V 0.3A DC fan supply
- Full international safety approvals & EMC standards

Standard Models

Model Number	Output Voltage	Output Current (Convection)	Output Current (Fan cooled)	Output Current (peak for 160mS)
PSY300S12	12V	16.67A	25.00A	33.33A
PSY300S18	18V	11.10A	16.60A	22.20A
PSY300S24	24V	8.33A	12.50A	16.66A
PSY300S30	30V	6.66A	10.00A	13.30A
PSY300S36	36V	5.55A	8.33A	11.10A
PSY300S48	48V	4.16A	6.25A	8.33A
PSY300S54	54V	3.70A	5.55A	7.40A

NOTE: Other models are available with output voltages from 9V to 57V DC.
These may be subject to minimum order quantities and specifications may differ to above depending on output voltage required. Consult sales office for further details.

POWER SOLVE

www.powersolve.co.uk
Email: sales@powersolve.co.uk
Tel: 44-(0)1635-521858 Fax: 44-(0)1635-523771

Figure 5: High-side bootloader

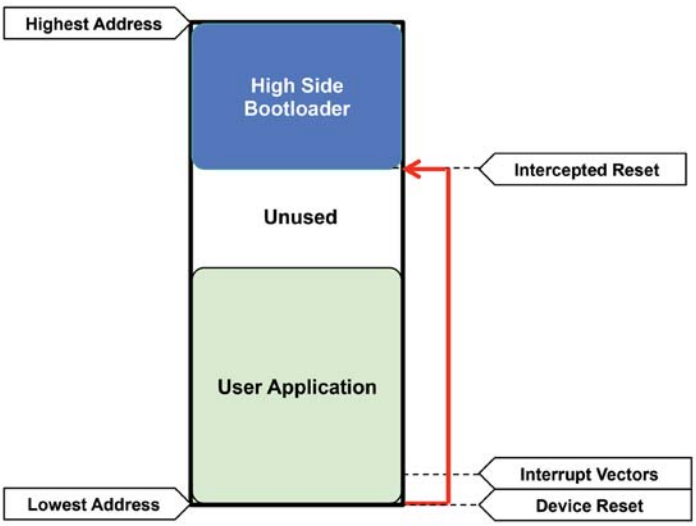

A USB connection is a different story. If a serial-to-USB bridge device (such as the MCP2221A) is not available yet an on-board USB peripheral is needed, a full USB library, such as those found in the Microchip Library for Applications (MLA) or MPLAB Harmony Integrated Software Framework, will be necessary.

If the Flash memory is truly at a premium, though, as is the case with minuscule PIC16F145x family, you might want to consider one of the exceptional projects shared on GitHub by two true wizards of PIC programming; see links [6] and [7] in the box.

MPLAB Code Configurator

Since the bootloaders' needs are so diverse, but they share a fundamental common set of building blocks for all PIC microcontrollers, the MPLAB Code Configurator (MCC) rapid development tool has been equipped with a new module (an extension) that automatically generates (low-side) bootloaders for most (approximately 400) currently-supported microcontrollers. See Figure 6 for a view of the configuration options available.

The code generated (at a click of a button) is quite compact and readable, so it is easy to extend and customise for any application.

A simple C# uploader application is available for download here: http://www.microchip.com/mymicrochip/filehandler.aspx?ddocname=en574038.

A Staple Of Applications

While Flash memory has been a staple of embedded applications for over 15 years, it is only with the advent of the IoT and the ubiquitous connectivity it brings to the embedded space that the need for true field-update capabilities has rocketed.

Writing and customising bootloaders for embedded applications can be challenging at times, but there are plenty of examples and new rapid development tools available to help. >

Figure 6: MCC bootloader configuration

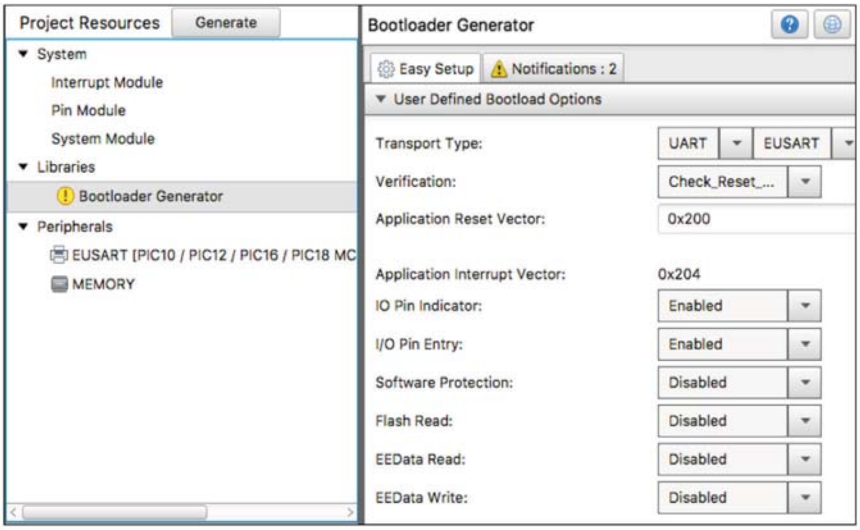

```
SECTIONS
{
 /* Boot Sections */
 .reset _RESET_ADDR :
 {
 KEEP(*(.reset))
 KEEP(*(.reset.startup))
 } > kseg1_boot_mem
 .bev_excpt _BEV_EXCPT_ADDR :
 {
 KEEP(*(.bev_handler))
 } > kseg1_boot_mem
 .dbg_excpt _DBG_EXCPT_ADDR (NOLOAD) :
 {
 . += (DEFINED (_DEBUGGER) ? 0x8 : 0x0);
 } > kseg1_boot_mem
```

Listing 1: A (cryptic) snippet of an MPLAB XC32 linker script example

```
 # 2. fix the reset vector to point to the BootStart vector
v[0..3]
 v = extend32bit([], info.BootStart/2)
 # low goto high Nop
 mem[0]=v[0]; mem[1]=0xEF; mem[2]=v[1];
mem[3]=0xF0+v[2]
```

Listing 2: Intercepting the reset vector of the PIC18

ADDITIONAL LINKS:

1. This is not Rocket Science – Lucio Di Jasio - Lulu.com - 2015 - ISBN:9781312907775
2. In 10 Lines of Code – Lucio Di Jasio – Lulu.com – 2016 – ISBN:9781329908031
3. Link to Micromedia Bootloader for Mac and Linux: https://bitbucket.org/luciodj/pic18hidbootloader
4. Microchip Bootloaders page: http://www.microchip.com/bootloader
5. Developers Help – Bootloaders : http://microchipdeveloper.com/mplabx:projects-loadable-bootloaders
6. A tiny USB CDC Bootloader : https://github.com/74hc595/PIC16F1-USB-Bootloader
7. A tiny USB DFU Bootloader : https://github.com/majbthrd/PIC16F1-USB-DFU-Bootloader
8. A Low-Side Bootloader for XPRESS : https://bitbucket.org/luciodj/serialbootloaderxpress
9. An I2C High-Side Bootloader: https://bitbucket.org/luciodj/pic16i2cblh
10. A Serial High-Side Bootloader: https://bitbucket.org/luciodj/pic16serhbl
11. A Simple Bluetooth Bootloader : https://github.com/luciodj/BlueBoot

E-paper displays in embedded systems

BY **DR DOGAN IBRAHIM**, PROFESSOR AT NEAR EAST UNIVERSITY, CYPRUS

Conventional displays are typically flat panels that work by emitting visible light. Their disadvantages include lack of visibility in bright sunlight and high power consumption.

E-paper (E-ink, Electronic Paper Display, EPD, or simply Electronic Paper) are new type displays that work by reflecting light. Their main advantage is that the image remains fixed after power is removed; as a result, they consume very little power.

E-paper displays are very clear, have wide viewing angles, can be large and flexible, and are comfortable to read in all ambient light conditions, with good contrast.

E-paper Evolution

E-paper was first developed in 1970 by Nick Sheridon at Xeros's Palo Alto Research Center who wanted to create a paperless office by replacing ordinary ink on paper with electronic ink. The first electronic paper, called Gyricon, was simple, consisting of tiny two-colour polythene spheres, embedded in transparent plastic sheet filled with oil so they rotate freely when subjected to electric fields. When fully rotated, the balls showed black, and when partially rotated they looked grey. By controlling the polarity and strength of the applied electric field, it was possible to display black or white pixels. The balls would remain in their most recent positions until another electric field was applied, thus requiring extremely low energy for operation, running for years from a small battery.

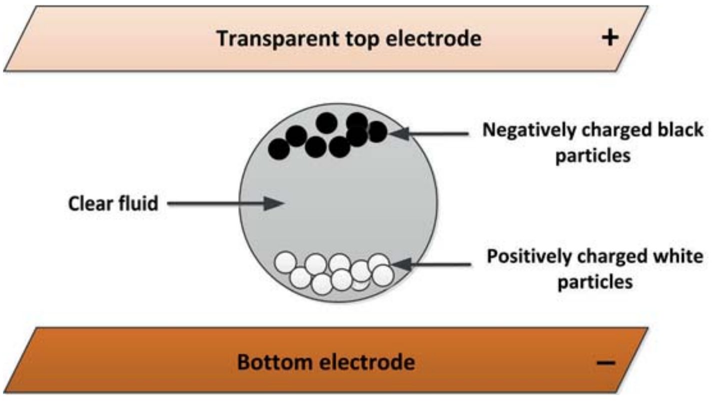

Figure 1: Electronic paper working principle

Early electronic papers were expensive and had limited resolution. Although the Gyricon project closed in 2005, many other companies have developed electronic papers, and now this technology has matured with the availability of fully-flexible, low-cost electronic papers that reproduce true colours. One popular and very successful application of electronic paper is the Amazon Kindle.

Present-day electronic papers are made of several million tiny capsules, each containing a different colour particle and different electric charge. In their simplest implementation, the particles are either black or white, with the white particles positively charged and the black negatively.

As shown in Figure 1, transparent electrodes are placed above and below the capsule array. When an electric field is applied, depending on field polarity, the negative black particles will be attracted by the positive polarity, and the positive white particles by the negative. The surface of the electronic paper will then display the required text or image.

Perhaps the biggest innovation in electronic paper technology is bright, true-colour electronic papers, showing up to 32,000 colours.

Applications

The market for electronic papers is projected to exceed $8.59bn by 2022. E-paper displays are flexible, so they can easily be folded and carried around. Their extremely-low power consumption makes them very desirable for portable devices; some smartphones like the Hisense A2 Pro and YotaPhone 3 already use them, with others expected to follow soon.

There are also E-paper-based computer monitors, such as the Dasung Paperlike, and laptops, such as the Onyx Boox. E-paper displays will find use in many more applications, including notice boards, traffic signs and billboards, among others; see Figure 2.

Figure 2: Examples of electronic paper displays

E-papers And LCDs

The choice between E-paper display and LCD depends on where and for how long the display will be used. In Kindle-type electronic reader applications the user may have to stare at the screen for many hours, which can cause eye-strain. Also, long battery life is usually an important requirement in such applications.

E-paper is probably the best choice for cases where a clear, sharp, steady and high-resolution image and wide viewing angle is needed, coupled with excellent contrast ratio and no glare.

LCD displays require frequent refreshing, for example 30 times every second, but E-paper displays are very efficient and can run for weeks on a single battery. Perhaps their biggest disadvantage is that they are hard to see in the dark, since there's no backlight. At present they are also more expensive than LCDs, and with slower response times.

Table 1 shows a comparison of the currently-available ordinary LCDs and E-paper displays.

CHARACTER LCD	E-PAPER DISPLAY
Medium power consumption	Ultra-low power consumption
Good contrast ratio	Excellent contrast ratio
Medium thickness	Very thin
Can have glare	No glare
Not flexible	Can be flexible
Medium size	Can be very large
Backlight required	No backlight
Not suitable for long hours reading	Ideal for long hours reading
Image flicker	Extremely steady image
Narrow viewing angle (60º)	Very wide viewing angle (180º)
Can be used in dark with backlight	Can't be used in dark
Suitable for fast video	Not suitable for fast video

Table 1 Comparison of LCDs and E-paper displays

Example E-paper Display System

Figure 3 shows a block diagram of a microcontroller-based thermometer system using an E-paper display. In this example,

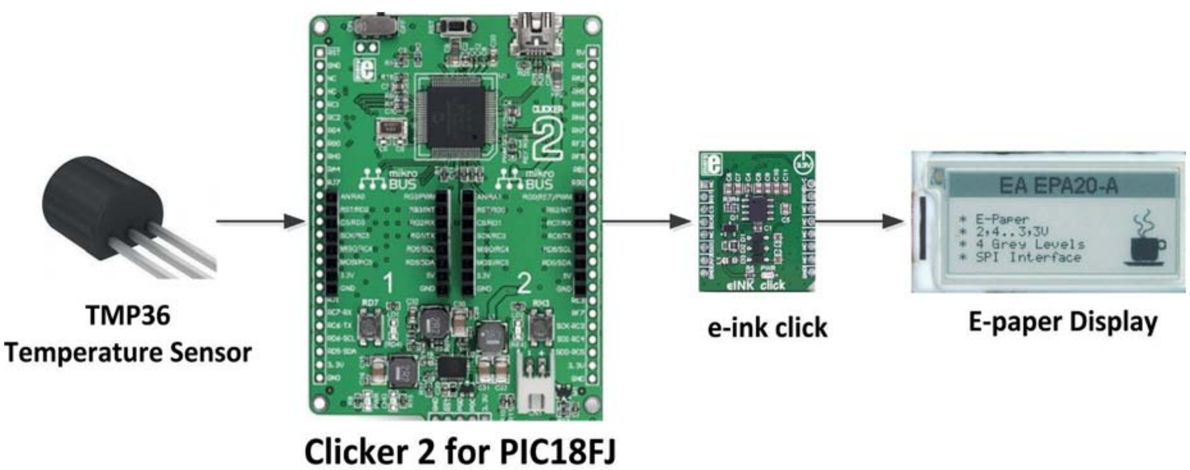

Figure 3: Block diagram of the example system

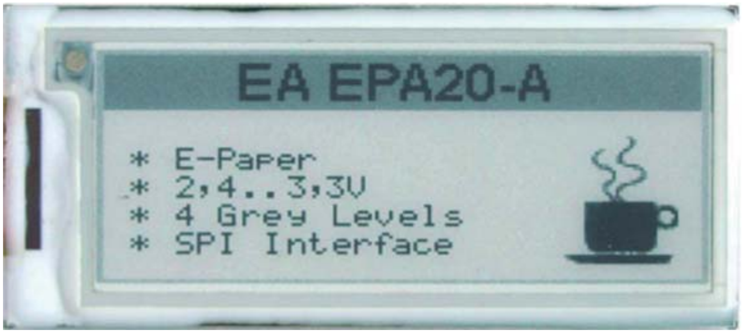

Figure 4: EA EPA20-A E-paper display

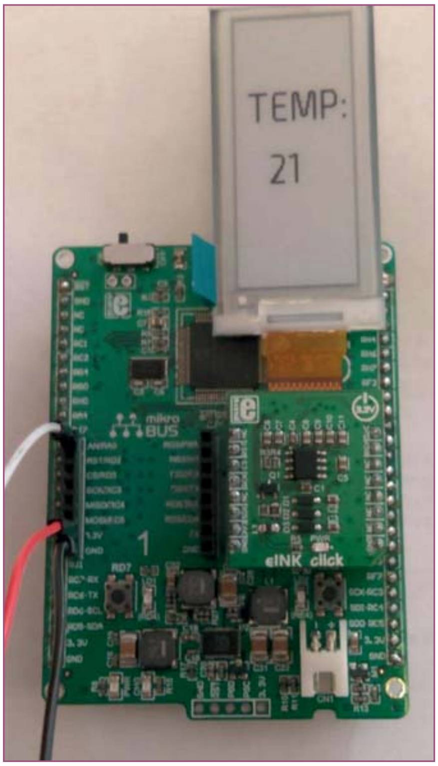

Figure 5: Temperature displayed on the E-paper display after removing power

an analogue TMP36-type temperature sensor chip measures the ambient temperature. This chip has three pins: GND, Vcc and Vo, where Vo is the analogue output pin, connected to one of the analogue input channels (AN0) of the PIC microcontroller.

TMP36 runs on 2.7-5.5V and measures temperatures between -40°C and +125°C with accuracy of ±2°C. The chip is calibrated to give an output voltage proportional to the measured temperature in °C, where the measured temperature is:

Temperature = (Vo – 500)/10

Vo is sensor output voltage in millivolts. Thus, for example, at 20°C the output voltage is 700mV, at 30°C the output voltage is 800mV, and so on.

As shown in Figure 3, this example system uses a Clicker 2 for PIC18FJ microcontroller development board, which incorporates a PIC18FJ50 medium-range microcontroller with two mikroBUS compatible sockets. The board also has the following basic features:

- 128kB flash program memory;
- 3904 bytes data memory;
- Bootloader;
- 48MHz operation (12MIPS);
- MicroUSB connector;
- Two LEDs and two pushbuttons;
- Reset button.

A mikroBUS compatible e-ink Clicker board with an E-paper display driver hardware is connected to mikroBUS socket 2 of the development board. The E-paper used in this example is the EA EPA20-A (Figure 4) small graphical display, connected to the display driver hardware with a short 24-pin flat cable.

EA EPA20-A has the following basic features:

- Pixels: 172 x 72;
- Diagonal size: 50.8mm;
- Viewing area: 48.16mm x 20.16mm;
- Interface: SPI;
- Colour: black and white;
- Operating voltage: 3.3V;
- Power consumption: 40mW.

In this system the ambient temperature is displayed on the E-paper every minute. Listing 1 is the complete program, which is based on the mikroC Pro for PIC IDE and language compiler. In addition to the E-paper library (called the e-ink library), the compiler includes several libraries to support different peripheral devices including UART, SPI, I2C, SD card, Bluetooth, Wi-Fi, and more.

At the beginning of the program, e-ink header files are included and the connections between display and microcontroller specified. Inside the main program, function *sysinit* is called to configure the input-output ports and SPI bus. The display is then configured to display black letters on white background, and the text EW (*Electronics World*) is displayed for three seconds. The remainder of the program runs endlessly.

Here, the ambient temperature is read from channel AN0, and is converted into degrees Centigrade. The temperature is then converted into a string in variable Txt, leading spaces removed and displayed on the E-paper at co-ordinates (20, 80). Text TEMP: is the heading, just above the temperature display.

The process repeats every minute.

Figure 5 shows the system with the ambient temperature (21°C in this example) displayed on the E-paper. The picture was taken with power removed from the system to show that the display is still active. >

```
*******************************************************

E-paper THERMOMETER EXAMPLE

A TMP36 type analogue temperature sensor chip
is used to read the ambient temperature using
a Clicker 2 for PIC18FJ type microcontroller
development board. The temperature is then
displayed on the E-paper every minute.

*******************************************************/

//
// E-paper (e-ink) header files
//
#include "eink.h"
#include "image.h"
#include "eink_font.h"
//
// E-paper connections
//
sbit EINK_C_CS at LATD1_bit;
sbit EINK_C_RST at LATD0_bit;
sbit EINK_C_DC at LATG0_bit;
sbit EINK_C_BSY at RB2_bit;
//
// Initialize the I/O ports and the SPI bus
//
void sysinit()
{
 TRISD1_bit = 0;
 TRISD0_bit = 0;
 TRISG0_bit = 0;
 TRISB2_bit = 1;
 SPI1_Init_Advanced( _SPI_MASTER_OSC_DIV4,
 _SPI_DATA_SAMPLE_MIDDLE,
 _SPI_CLK_IDLE_HIGH, _SPI_LOW_2_HIGH );
}
//
// Start of MAIN program. Read and display the
ambient temperature
//
void main()
{
 unsigned int Temp;
 char Txt[7];
 float mV, Temperature;
 sysinit();
 eink_init();
 Delay_Ms(1000);
//
// Display black letters on white background
//
 eink_fill_screen(EINK_COLOR_WHITE);
 eink_set_font(guiFont_Exo_2_Condensed21x32_
Regular,
 EINK_COLOR_BLACK,FO_HORIZONTAL );
 eink_text("EW",20,40);
 Delay_Ms(3000);
//
// Read the temperature and display every minute
//
 while(1)
 {
 eink_fill_screen(EINK_COLOR_WHITE);
// Display black on white
 eink_text("TEMP:",8,40);              //
Display heading
 Temp = ADC_Read(0);              // Read
temperature
 mV = 3300.0*Temp/1024.0;              //
Temperature in mV
 Temperature = (mV - 500.0)/10;              //
Temperature in C
 Temp = (int)Temperature;              //
Convert to integer
 IntToStr(Temp, Txt);              //
Convert to string
 Ltrim(Txt);              // Remove spaces
 eink_text(Txt,20,80);              //
Display temperature
 Delay_ms(60000);              // Wait 1
minute
 }
}
```

Listing 1: Program listing of the example system

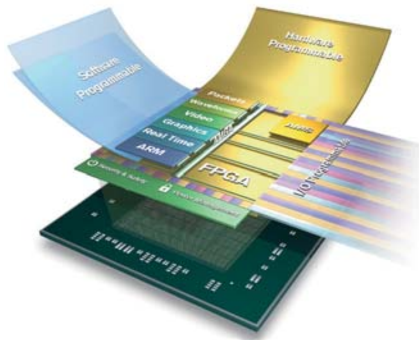

Vision beyond the visible

BY **GILES PECKHAM** AND **ADAM TAYLOR** OF XILINX

One advantage of embedded vision systems is their ability to observe wavelengths outside those visible to humans, providing superior performance in many applications, from low-light vision to scientific imaging and analysis.

While imaging systems at higher wavelengths, including x-rays and ultraviolet light, are used for scientific applications such as astronomy, infrared (IR) wavelengths are most often used in industrial, automotive and security applications. Since IR imagers sense the background thermal radiation, they don't need scene illumination and can 'see' in total darkness, which is ideal for automotive and security applications.

In the industrial space, IR systems can also be used in thermo-graphic applications to accurately measure the temperature of the scene contents. For example, in renewable energy, thermal imagers are combined with drones to monitor the performance of solar arrays and detect early failures due to elevated temperatures of failing elements.

IR Imagers

Working outside the visible range requires the correct selection of the imaging device. If the system operates in the near-IR spectrum or below, developers can use CCDs (Charge Coupled Devices) or CMOS CIS (Complementary Metal Oxide Semiconductor Image Sensors). However, for the infrared spectrum, specialised IR detectors are required.

The need for specialised sensors in the IR domain is in part due to the excitation energy required for silicon-based imagers such as CCD or CIS. These typically require photon energy of 1eV to excite an electron, but at IR wavelengths photon energies range from 1.24meV to 1.7eV. As such, IR imagers tend to be based on HgCdTe or InSb, which have lower excitation levels and are often combined with a CMOS readout IC, called a ROIC, to control and read the sensor.

IR systems fall into two categories, cooled and uncooled. Cooled thermal imagers use image sensor technology based on HgCdTe or InSb semiconductors. To provide useful images, a thermal imager requires a cooling system to reduce the temperature of

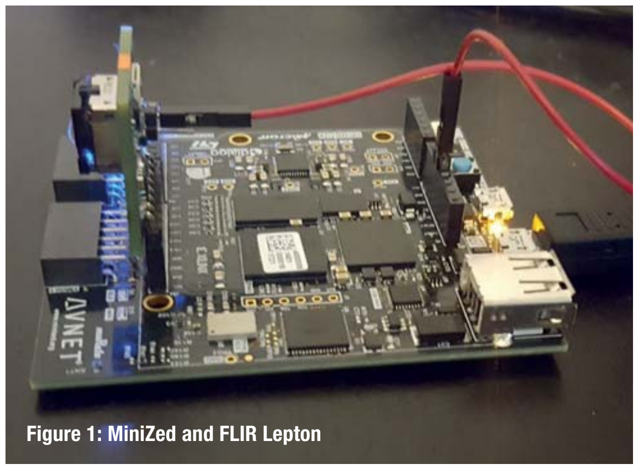

Figure 1: MiniZed and FLIR Lepton

its sensor to 70-100 Kelvin, also reducing the generated thermal noise to below that of the scene contents. But, using a cooled sensor increases design complexity, cost, weight and, importantly, the time required to reach operating temperature and generate a useable picture.

Uncooled IR sensors can operate at room temperatures and use micro-bolometers in place of an HgCdTe or InSb sensor. A micro-bolometer works by changing each pixel's resistance when IR radiation strikes it; the resistance changes define the temperatures in the scene.

Typically, micro-bolometer-based thermal imagers produce lower resolution images than cooled imagers, but they simplify system design, making it lighter and less costly to develop. This is why many industrial, security and automotive applications use uncooled image sensors like the FLIR Lepton.

Developing an uncooled thermal imager can be challenging, requiring a flexible interface to connect the device and display, while implementing any additional image processing of the video stream. Equally important is that many of these devices are handheld or power-constrained, so power efficiency also becomes a significant factor.

Example Architecture

The FLIR Lepton is a thermal imager that operates in the long-

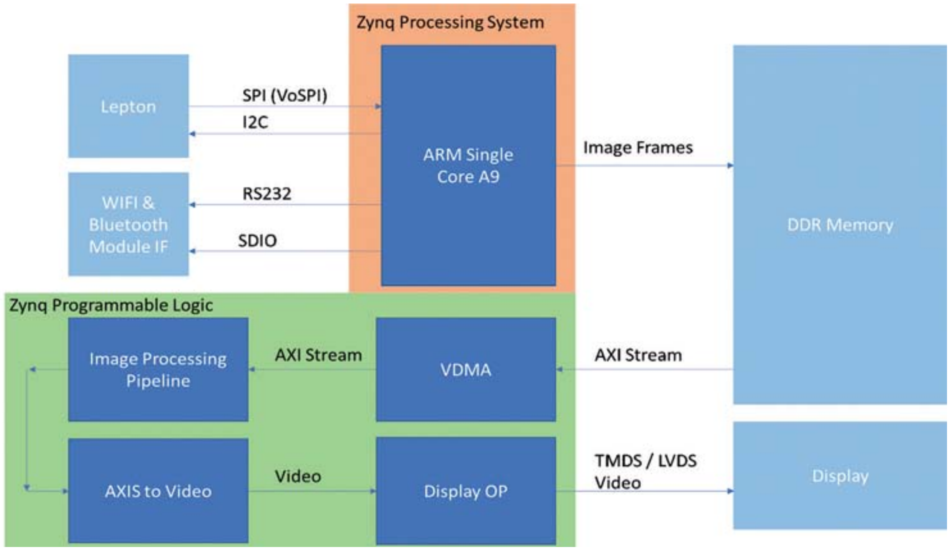

Figure 2: The solution's high-level architecture

wave IR spectrum. It is a self-contained camera module with a resolution of 80 x 60 pixels (Lepton 2) or 160 x 120 pixels (Lepton 3). Configuration of the Lepton is via an I2C bus, while the video output uses a Video over SPI (VoSPI) protocol. These interfaces make it ideal for many embedded systems that image in the IR region.

One example combines the Lepton with a Xilinx Zynq Z7007S device mounted on a MiniZed development board. Since the MiniZed board supports WiFi and Bluetooth, it is possible to create both IIoT/IoT applications and traditional imaging solutions with a local display, in this case a 7-inch touch display. This example creates a design that interfaces with the FLIR Lepton and sends the video to a local display.

To create a tightly-integrated solution, designers can use the processing system (PS) of the All Programmable Zynq SoC to configure the Lepton via the I2C bus. The PS can also provide an interface to the radio module for WiFi and Bluetooth communication for future upgrades, while the programmable logic is used to receive VoSPI, perform direct memory access with DDR and produce video. See the high-level architecture of the solution in Figure 2.

Within the image processing pipeline, designers can instantiate custom image-processing functions generated with High-Level Synthesis (HLS) or by using pre-existing IP blocks, such as the Image Enhancement core that provides noise filtering, edge enhancement and halo suppression.

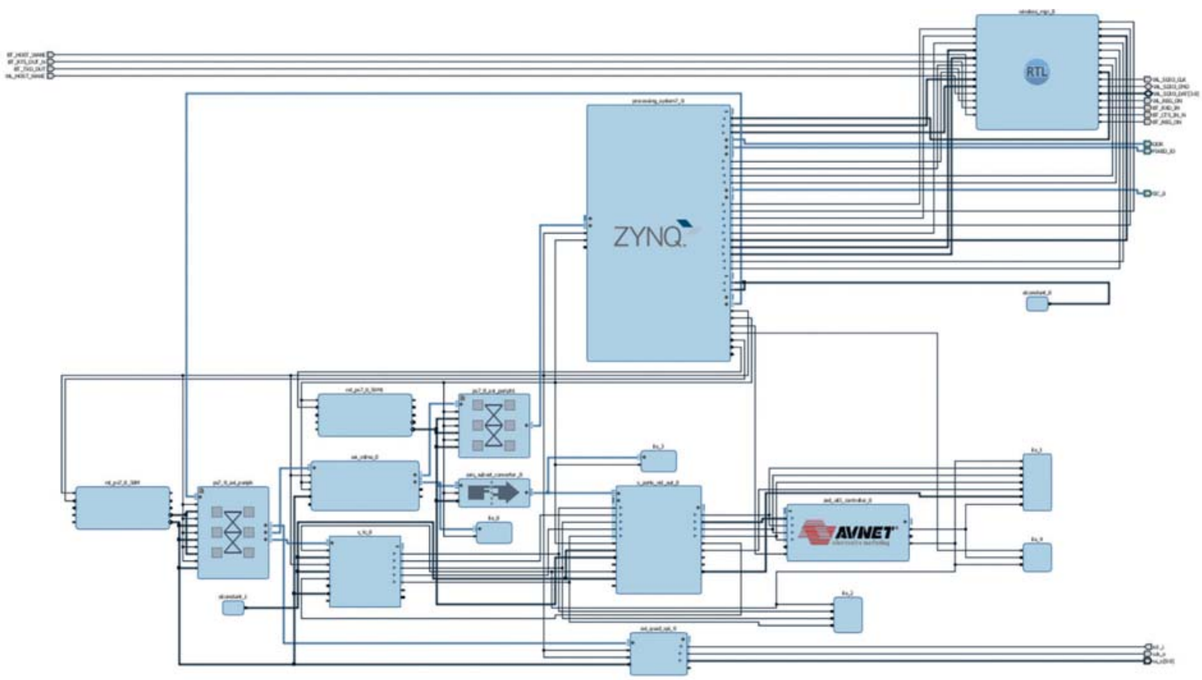

Figure 3: Detailed hardware design in Vivado

Figure 4: FLIR Lepton output – the residual fingerprints on a cold glass are very clear, demonstrating the sensitivity of the detector

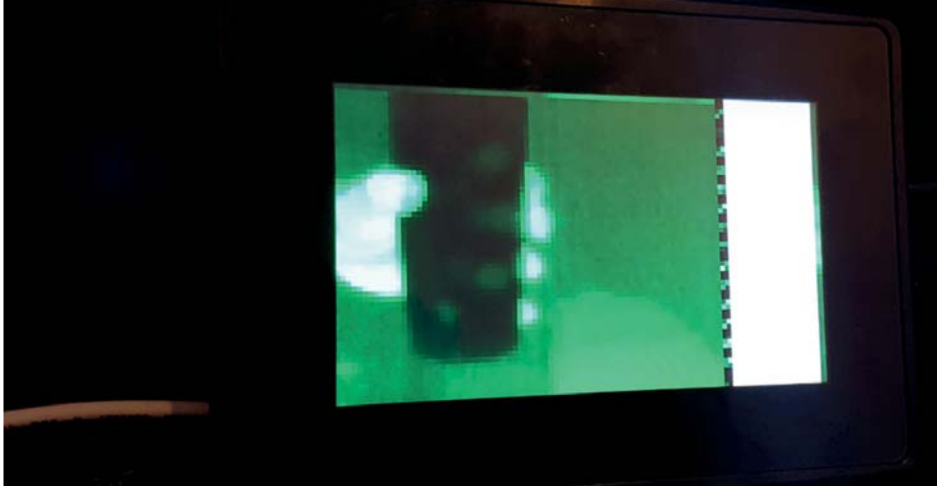

Since this high-level architecture requires translation into a detailed design within Vivado, the following IP blocks are used to create the hardware solution:

- **Quad SPI Core** – Configured for single-mode operation, receives the VoSPI from the Lepton.
- **Video Timing Controller** – Generates the timing signals for the output display.
- **VDMA** – Reads an image from the PS DDR into a PL AXI stream.
- **AXI stream to Video Out** – Converts the AXI-streamed video data to parallel video with timing sync provided by the Video Timing core.
- **Zed_ALI3_Controller** – Display controller for the 7-inch touchscreen display.
- **Wireless Manager** – Provides interfaces to the radio module for Bluetooth and WiFi. While not used in this example, to include this module within the hardware design adds wireless communications using software development only.

When these IP blocks are combined with the Zynq processing system and the necessary AXI interconnect IP, the result is a detailed hardware design as shown in Figure 3.

Software Definition

Most of the IP blocks included in the Vivado design require configuration using application software from the software development kit (SDK). This provides flexibility to change operational parameters as the product evolves, for example to accommodate a larger display or change the sensor from Lepton 2 to Lepton 3.

For this example, no operating system is required; the application software configures from the video timing controller (800 pixels x 480 lines), along with the video direct memory access controller, to read frames from the memory-mapped DDR and convert them into an AXI stream for image-processing.

Following initialisation of the IP blocks, the applications software performs the following:

- It configures the FLIR Lepton to perform automatic gain control.
- It synchronises with the VoSPI data to detect the start of a valid frame.
- It applies a digital zoom to scale up the image to efficiently utilise the 800pixels-by-480line display. This can be achieved by outputting each pixel either eight or four times, depending on sensor selection.
- It transfers the frame to DDR memory. Since the FLIR Lepton only produces 8-bit data when ACG is enabled, this is mapped to the green channel of the RGB display.

When the completed programme is executed on the MiniZed with the FLIR Lepton and connected to a 7-inch display, the output of the FLIR can be seen very clearly.

CMOS vs LVCMOS: which is the best for your application?

BY **ROB RUTKOWSKI**, BLILEY TECHNOLOGIES

One of the most important choices an RF engineer will make is to decide what type of output signal is best for their project. I wrote about CMOS in last month's column; there are different variations of it, some are more appropriate for some applications than others. Here I'll discuss the benefits of Low-Voltage Complementary Metal Oxide Semiconductors, otherwise known as LVCMOS.

CMOS And LVCMOS

There are many advantages of CMOS over other type output signals, the biggest being its low power requirements. CMOS clocks are generally inexpensive and keep phase noise to a minimum. They are well-suited to digital circuit designs, particularly those with shorter trace lengths.

CMOS integrated circuits (ICs) were first developed in the 1960s, and one of their distinguishing features is their ability to operate over a wider range of supply voltages – from 3V to 15V. As the technology advances, there's a shift toward even lower supply voltages.

Manufacturers began to develop smaller circuit designs to cut costs and improve performance, which is accompanied by a further reduction in power, thanks to a new low-voltage class of CMOS ICs.

The Joint Electron Device Engineering Council (JEDEC) defined LVCMOS supply voltage and interface standards as follows:

- 3.0-3.3V;
- 2.5V ± 0.2V (normal range) and 1.8-2.7 V (wide range);
- 1.5V ± 0.1V (normal range) and 0.9-1.6V (wide range);
- 1.2V ± 0.1V (normal range) and 0.8-1.3V (wide range);
- 1.0V ± 0.1V (normal range) and 0.7-1.1V (wide range).

Right For The Application?

LVCMOS output signals are used for certain low-powered medical imaging equipment, as well as portable testing and measurement devices, industrial testing equipment and networking and communication systems; LVCMOS is well suited to both wireless and wired infrastructure.

Despite its widespread use, however, is it the best output for your application?

The short answer is "it depends"; it specifically depends on the power availability for the application. If there's access to more power and the application requires it, then going with a higher-voltage CMOS clock makes more sense. If power is limited and you are trying to reduce power costs, then LVCMOS is the way forward.

Despite CMOS technology advantages, it's important to get it right the first time during the design stage when deciding what signal output to choose. The decision will also depend on design priorities such as reduced phase noise, lower power consumption, and so on. It can be a tough choice, and making the wrong one can result in wasted time and money. ●

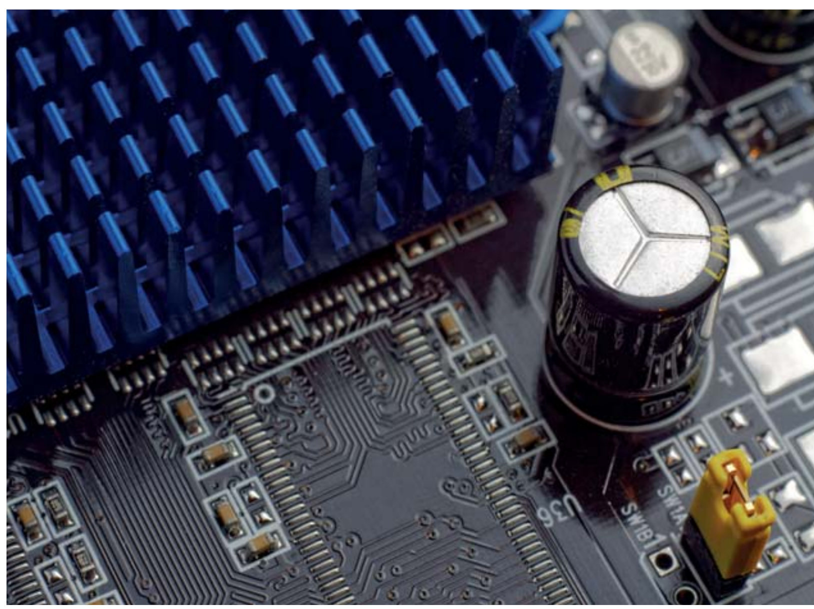

Figure 1: One of the most distinguishing features of CMOS ICs is their ability to operate over a wider range of supply voltages than other technologies

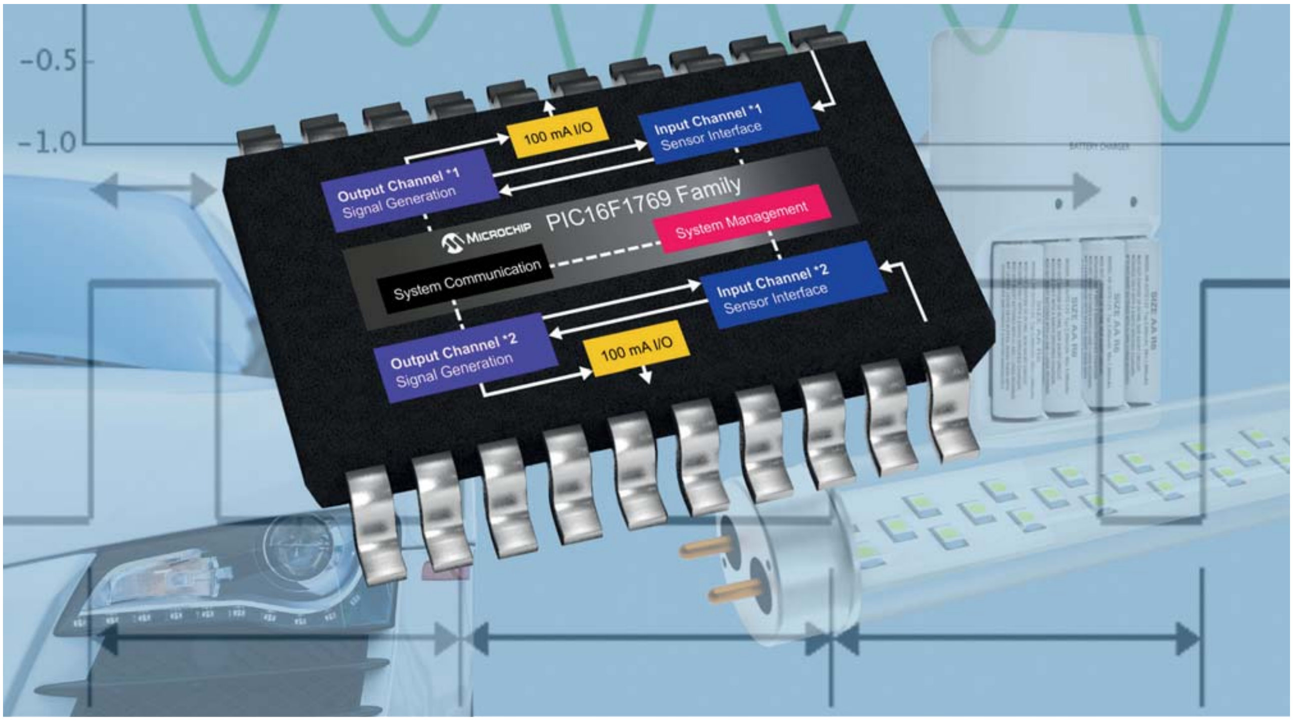

RAMPING UP, OR DOWN, OR A BIT OF BOTH

KRISTINE ANGELICA SUMAGUE FROM MICROCHIP TECHNOLOGY EXPLAINS HOW TO USE A PROGRAMMABLE RAMP GENERATOR TO CREATE A VOLTAGE RAMP SIGNAL

A voltage ramp signal can be used in a circuit that requires a linear change of voltage. It is commonly used as a reference signal, slope compensator or voltage sweep generator. Such a signal can be created using the Programmable Ramp Generator (PRG) peripheral available on many Microchip PIC microcontrollers, without any processor overhead. The PRG can produce a falling or rising ramp, or an alternating rising-falling ramp triggered from different input sources.

The PRG in falling ramp mode, for example, can be used as a slope compensator in a DC-DC converter operating in continuous current mode. The decaying ramp produced by the PRG prevents sub-harmonic oscillations and helps stabilise the output when the duty cycle exceeds 50%.

In Figure 1, the PRG's ramp-generation function works by driving a constant current into the internal capacitor; the resulting voltage is added to or subtracted from the voltage input source. The mode of operation of the ramp output relies mainly on control of the internal analogue switches. The interval between when the ramp starts and stops is determined by the input timing sources.

“The mode of operation of the ramp output relies mainly on control of the internal analogue switches

Input Timing Sources

The PRG combines two selectable, independent, timing sources to generate control timing for its ramp output. These sources can be an external input from the PRGxR and F pins, or outputs from other peripherals. The rising input is selected by setting the Set Rising Timing Source Select (RTSS) bits in the RTSS register, while the set falling input is selected by setting the set Falling Timing Source Select (FTSS) bits in the FTSS register.

The polarity of timing sources is selected by setting the Fall Event Polarity (FPOL) and Rise Event Polarity (RPOL) select bits in the CON1 register.

Aside from the selectable timing input sources and the polarity event, the input source detection method can also be selected. The two event detection methods for PRG are level- and edge-sensitive. Rising and falling input detection are selected by setting the set rising input mode (REDG) and set falling input mode (FEDG) select bits in the CON0 register.

In general, edge-sensitive operation is useful when timing inputs are derived from periodic sources, whereas level-sensitive operation inputs are derived from voltage thresholds.

The timing sources for the PRG may vary from device to device. Some of the available peripherals that can be used as PRG's timing sources are comparator, PWM (Pulse-Width Modulation) and CCP (Capture, Compare, PWM) output. The peripheral must be configured beforehand and selected as the PRG's timing source.

Voltage Input Source

The PRG's voltage input source serves as a voltage reference to the linear ramp output. The input source can be any of the following: external source from the PRG's IN0 or IN1 pins; the buffered output of the internal Fixed Voltage Reference (FVR); or one of the internal digital-to-analogue converters (DACs).

The op-amp outputs share the IN0 and IN1 pins so the reference signal can be buffered by the op-amp by enabling both the op-amp and selecting the corresponding IN pin. Reference sources are selected by setting the voltage input select bits in the INS register.

Current Source/Sink

The programmable current on the PRG has a vast selection of source-sink currents to configure the desired PRG output slope rate. In applications that require a steep voltage rate at the PRG output, a high-current setting must be selected. The constant ramp current is selected with the source-sink set bits in the CON2 register.

Mode Selection

The PRG can be operated in one of three voltage ramp generator modes: falling ramp generator – slope compensation; rising ramp generator; or alternating rising-falling ramp generator. The modes are selected by setting the programmable ramp generator mode selection bits of CON0. The PRG output for each mode is controlled by the SW1, SW2 and SW3 internal analogue switches; SW1 discharges the internal capacitor when the switch is closed, while SW2 and SW3 connect the other side of the capacitor to the programmable current source and current sink, respectively.

Switching SW2 and SW3 dictates the flow of charge to the internal capacitor. These switches toggle depending on the configured mode. In the falling ramp mode, SW2 is open, SW3 is closed and SW1 toggles on and off. Since SW3 is closed while SW1 is open, the internal capacitor is charged by a current sink. The voltage across the capacitor is subtracted from the voltage input source and produces a falling ramp output at the configured slope rate.

Rising ramp mode has the same operation except for the SW2 and SW3 switching states. In this mode, SW2 is closed

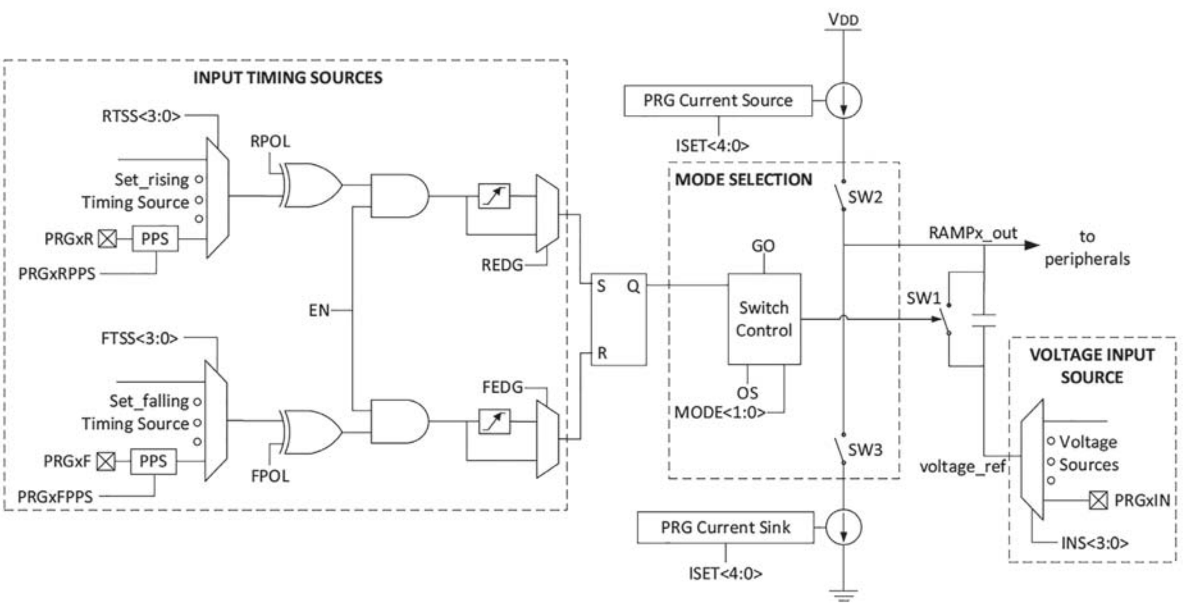

Note: SW1 discharges the internal capacitor.
SW2 is closed and SW3 is open during Rising Ramp Generator mode.
SW3 is closed and SW2 is open during Falling Ramp Generator mode.
SW2 and SW3 alternate switching during alternating Rising/Falling Ramp Generator mode.

Figure 1: Simplified PRG block diagram

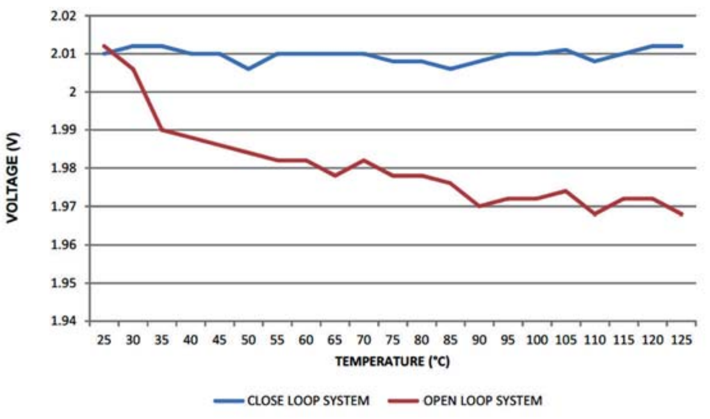

Figure 2: PRG average voltage versus temperature

and SW3 is open. When SW2 is closed while SW1 is open, the internal capacitor is charged by the current source, producing a rising ramp output.

In the alternating rising and falling ramp mode, SW1 remains open and SW2 and SW3 toggle alternately. This means when SW2 is closed, SW3 is open and vice versa. Since SW1 remains open in this mode, the reference voltage has no effect on the PRG output because there will be no discharge state to take it to the reference voltage. SW2 and SW3 toggling alternately will connect the internal capacitor to either source or sink current to charge the capacitor from one direction to another, producing an alternating rising and falling ramp on the PRG output.

One difficulty with alternatively switching SW2 and SW3 is that the source and sink currents that flow through the internal capacitor do not exactly match due to several factors, including parasitic resistance of the capacitor, noise, production variance and temperature. This greatly affects the performance of the PRG in an open-loop system, which determines the PRG's average output voltage to drift over time. This is an inherent limitation of the system, and hence impossible to trim out.

However, the voltage drift can be reduced by creating a feedback loop on the PRG. The PRG output is tied to one of the comparator inputs, while the comparator output acts as one of the PRG timing inputs to maintain peak voltage level at the PRG output. Hence, the average voltage of the PRG output in a closed-loop system will have a small drifting deviation than the open-loop system.

To see the PRG's average voltage drift in alternating ramp generator mode, it can be subjected to increasing ambient temperature. This accelerates the effect of temperature on the performance of the PRG output.

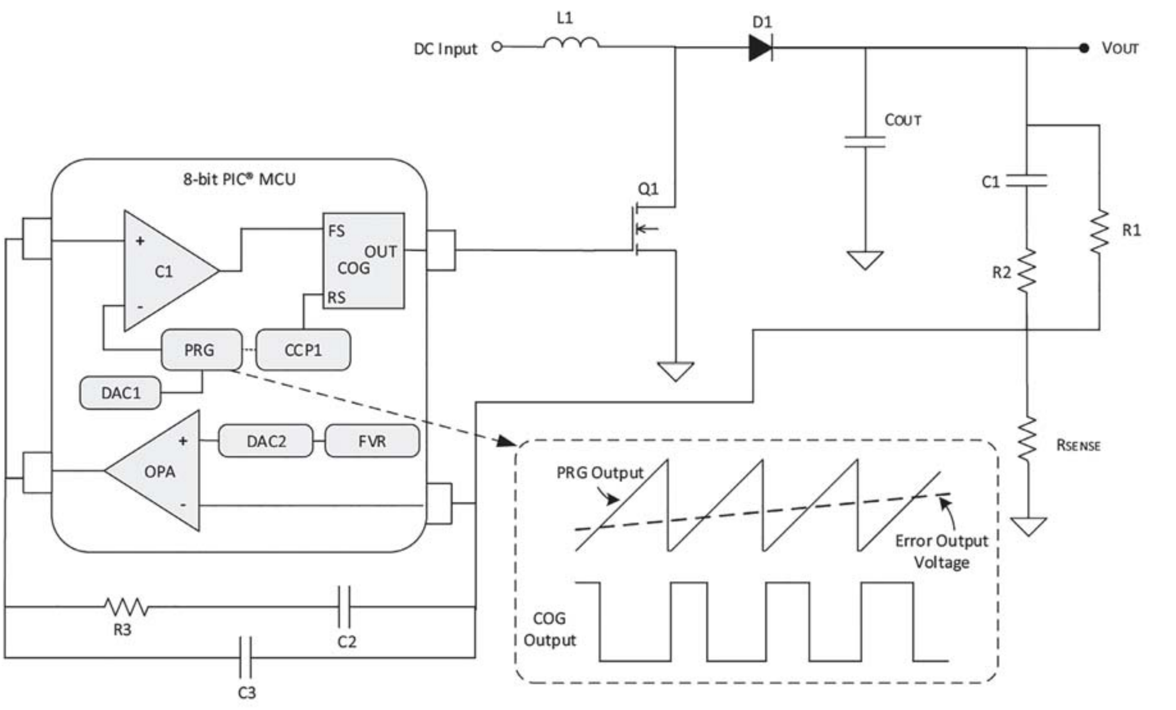

Figure 3: DC-DC converter using voltage mode

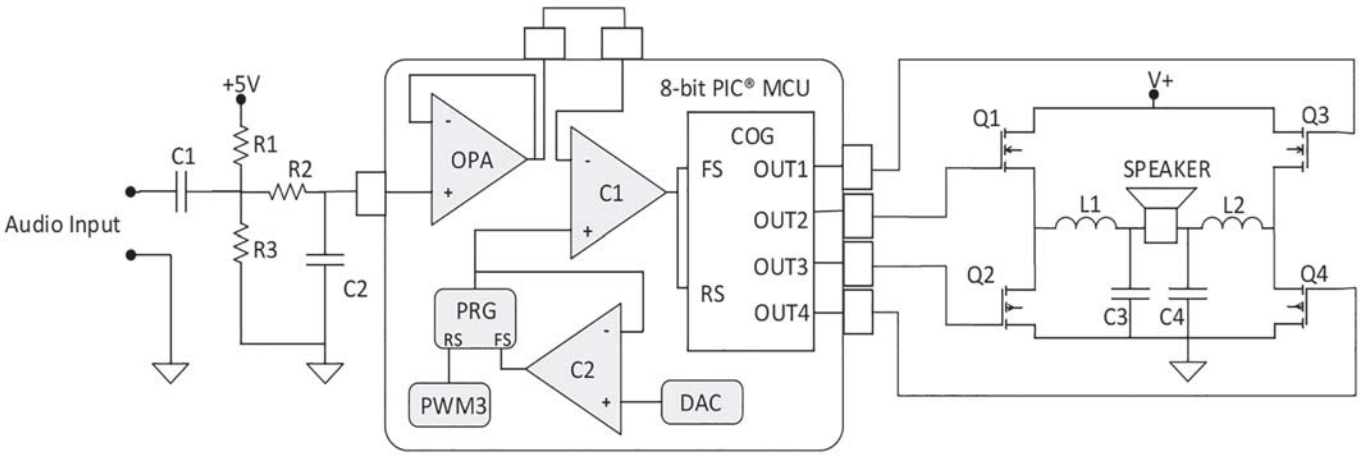

Figure 4: Full-bridge class D amplifier

As shown in Figure 2, there is significant voltage deviation with temperature when the PRG operates in an open-loop system. However, this deviation produces almost constant average voltage when a closed-loop system is used.

One-Shot Timer

The PRG module has an optional one-shot timer that minimises capacitor discharge time for both rising and falling ramp modes and also minimises rising or falling ramp duration in the alternating ramp mode.

In the rising and falling ramp modes, the one-shot timer ensures the capacitor is discharged by holding its shorting switch SW1 closed for at least one one-shot period (typically 50ns), whereas in alternating ramp mode, both rising and falling ramps persist for a minimum of one one-shot period.

Edge-sensitive timing inputs that occur during the one-shot period are ignored, while level-sensitive timing inputs that occur during and extend beyond the one-shot period are suspended until the end of the one-shot time. The one-shot timer is enabled by setting the OS bit of the CON0 register.

Applications

As discussed, the Programmable Ramp Generator (PRG) peripheral on many PIC microcontrollers can create a voltage ramp signal for use as a reference signal, slope compensator or voltage sweep generator.

Along with its use in DC-DC converters mentioned earlier, a PRG can also be used to regulate the output of a Switch-Mode Power Supply (SMPS) by implementing voltage mode control (Figure 3).

As with peak current control mode, voltage mode control output regulation can be achieved by adjusting the PWM duty cycle that drives the switching of the Metal-Oxide Semiconductor Field-Effect Transistor (MOSFET). However, instead of comparing the output error with the derived inductor current to adjust the PWM's duty cycle, the output error in voltage mode control is compared with a reference ramp voltage. The rising ramp signal generated by the PRG in a rising ramp mode can be used as the reference ramp voltage.

In Figure 3 the output error measured by the OPA error amplifier is compared with the PRG's rising ramp signal.

While the rising ramp voltage still does not reach the error voltage, the duty cycle of the complementary output generator (COG) output is increasing. But, once the rising ramp signal reaches the output error voltage, the duty cycle of the COG is terminated.

Another application (Figure 4) sees the alternating rising and falling waveform produced by the PRG used as a reference signal in a half-bridge or full-bridge class-D amplifier. In this application, a closed-loop PRG configuration addresses the average voltage problem in alternating ramp mode.

The PRG's alternating ramp output is compared with the analogue audio input signal through an internal comparator with inverted output. The comparator's output produces pulse waveforms directly proportional to the instantaneous values of the audio signal. These pulse waveforms are fed to the COG whose complementary PWM outputs drive Q1 and Q4 are high, and Q2 and Q3 low, or vice versa. Finally, a low-pass filter is used to remove the carrier frequency and recreate the analogue audio signal.

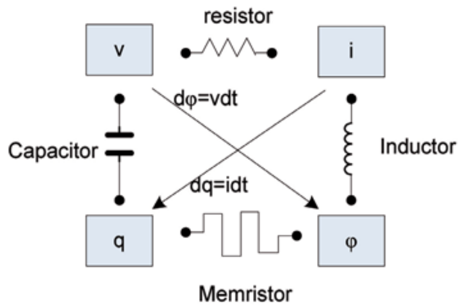

Figure 1: The fundamental circuit components and their relationships

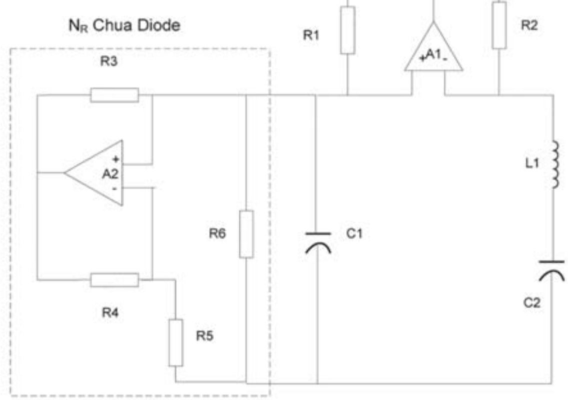

Figure 2: The four-element Chua circuit

SIMULATION AND APPLICATION OF MEMRISTOR-BASED CHUA'S CHAOTIC CIRCUIT

HASAN GULER AND **TURGAY KAYA** FROM FIRAT UNIVERSITY IN TURKEY DESCRIBE A MEMRISTOR-BASED CHAOTIC CIRCUIT IN THE LABVIEW VIRTUAL INSTRUMENT ENVIRONMENT

In principle, there are only four basic circuit variables: current (I), voltage (V), charge (q) and magnetic flux (φ). Relations between I and V, I and φ, and V and q are defined via components like resistors (R), inductors (L) and capacitors (C), respectively. However, until 1971, when Professor Leon Chua at Berkeley defined the memory resistor, also known as 'memristor', the relationship between q and φ was left undefined; see Figure 1.

A memristor is an electrical component that limits or regulates the flow of electrical current in a circuit and remembers the amount of charge that previously flowed through it. Being non-volatile, i.e. it retains memory without power, the memristor is considered a form of storage device, and thus an important technology.

The electrical characteristics of a memristor are memristance and memductance, which are inverse of each other, and the unit for memristance is the same as for resistance.

Although the memristor has long been a subject of interest to scientists and engineers, a working memristor did not appear until 2008, developed by Hewlett-Packard (HP) engineers. To date, memristors are still not commercially available because of their high production costs, so many studies about memristor-based systems are implemented only by using emulators and simulation tools such as SPICE.

Because memristors have naturally nonlinear behaviour, they can be successfully applied to chaotic circuits, which are nonlinear dynamical systems, highly sensitive to initial conditions.

One such system is the simple Chua circuit, which exhibits classic chaos behaviour. This roughly means that it is a "nonperiodic oscillator", producing a waveform that, unlike with an ordinary oscillator, never repeats. Chaotic circuits are widely used in secure communications, among other applications.

The Chua Circuit Model

We developed a Chua-memristor-based chaotic circuit using the LabVIEW environment by National Instruments (NI). LabVIEW is graphic-based software platform, supported by data acquisition cards (DAQs) and CompactRIO (c-RIO) embedded controllers, widely used in advanced control and monitoring systems.

In the study, we derived mathematical equations of the Chua circuit, and by using the LabVIEW environment observed the circuit's chaotic behaviour. We then developed a real-time application of this system using the NI's 6009 DAQ device.

The nonlinear resistor NR, which in this circuit is called Chua's diode, is replaced with a memristor to implement the circuit as chaotic. The effect of the A1 op-amp is set to -k, where k is the coefficient used to show the op-amp effect in the circuit; see Figure 3. The values of the basic circuit elements for this system were selected to be C1= 40nF, C2 = 120nF, L1 = 15mH and k = 7.55.

The circuit's memductance, named voltage-controlled ideal memristor, is W(φ). The memristor's piecewise linear (PWL) function used for easy calculation of the mathematical equations is shown in Figure 4.

LabVIEW-Based Modelling

We used the LabVIEW v.12.0f3 (32-bit) service pack 1 (SP1) for Windows to simulate the four-element memristor-based chaos

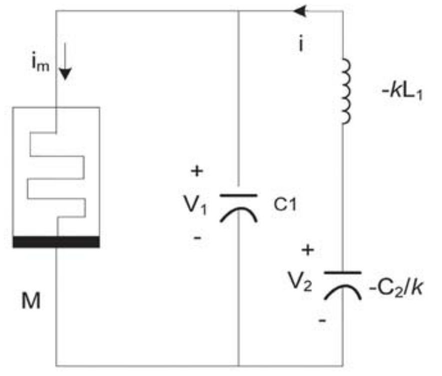

Figure 3: The implementation of Chua's circuit with basic elements

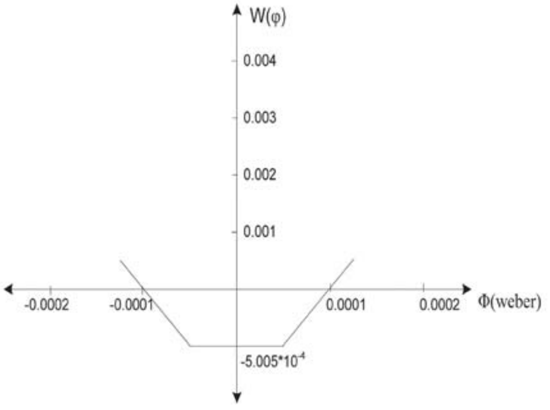

Figure 4: Memristance function W(ϕ)

circuit. We chose LabVIEW because it is a graphical, easy-to-use interface, enabling easy implementation of real-time circuits with DAQ devices and cRIO components.

Our experimental system is shown in Figure 5. On the front panel of the virtual instrument, there are three tabs shown – real attractors, normalised attractors and instant values of attractors; see Figures 6-7.

An attractor is a set of numerical values toward which a system tends to evolve. A chaotic attractor is a set of states in a system's state space with special properties, and a real attractor shows the real values of a system. In our system, the obtained real values are between -12.5V and 15V, and our DAQ card's output range is 0-5V. This means these values must be normalised in a block diagram to see the oscilloscope's screen. Instant values of I, V and φ show the instant values constituting the attractors.

We used a control and simulation loop and the ODE45 (Ordinary Differential Equation) solver method to implement the system, with initial conditions of start time = 0s, final time = 0.1s, φ = 0, V1 = 0.1, I = 0 and V2 = 0. Memristor-based nonlinear systems may take longer simulation times, which is why we used the ODE45, since it handles long, numerical simulations and complex calculations.

Four different attractors graphs were shown on the virtual instrument's front panel of the developed program: V1-V2, V1-I, V1-φ and φ-I; see Figures 6 and 7.

Real-Time Application

We used the NI-6009 DAQ device to investigate the chaotic behaviour of the four-element memristor-based circuit.

As discussed earlier, because the analogue output voltage range of the DAQ card is 0-5V, and the instant values of the variables are greater, the instant values must be normalised to show the chaotic behaviour of this circuit in the analogue outputs of the DAQ.

The normalisation was done in a block diagram, and both the obtained real and normalised attractor figures were shown on the front panel. Figure 8 shows the real, normalised

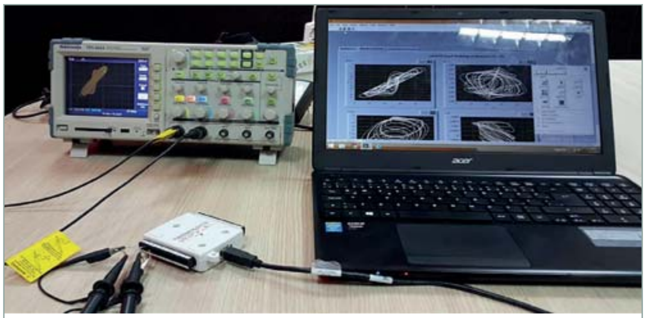

Figure 5: Experimental setup

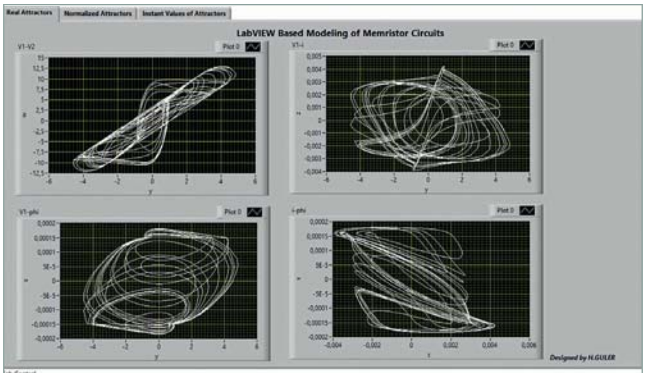

Figure 6: LabView panel for real attractors

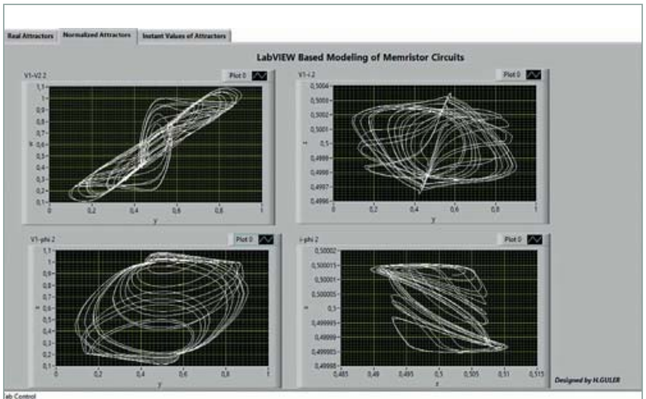

Figure 7: LabView panel for normalised attractors

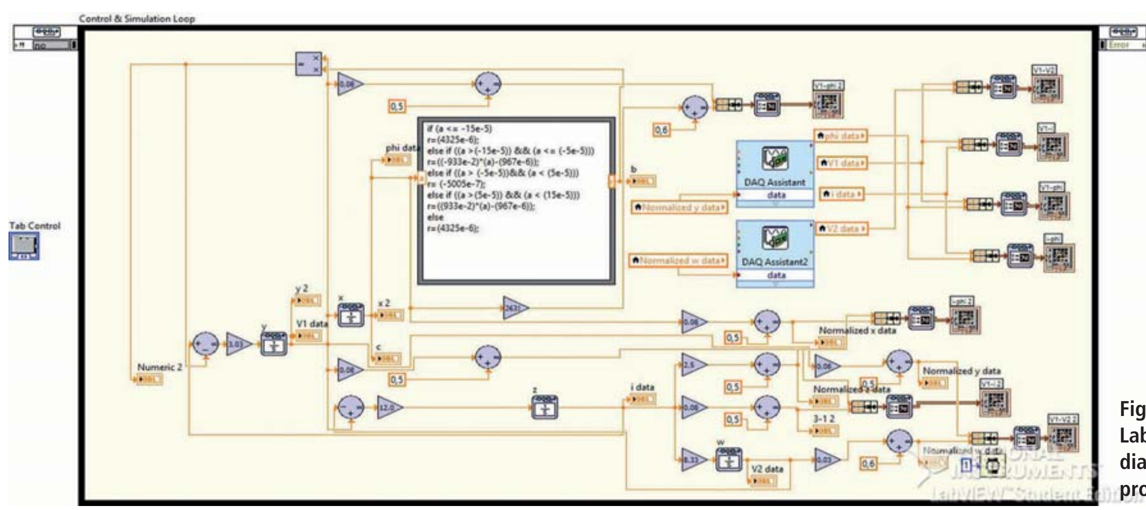

Figure 8: LabView block diagram of the program

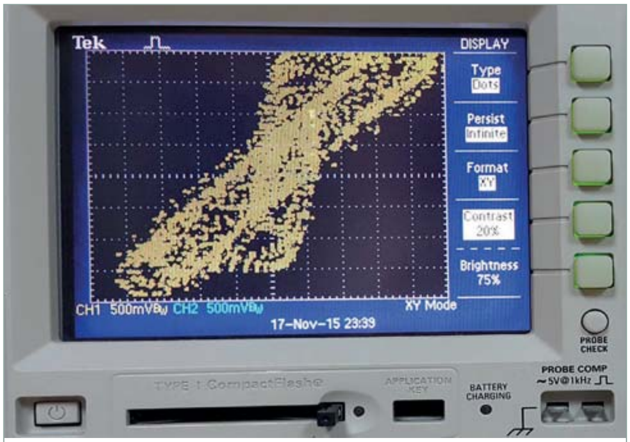

Figure 9: Real-time display for V2 vs V1

Figure 10: Real-time display display for I vs V1

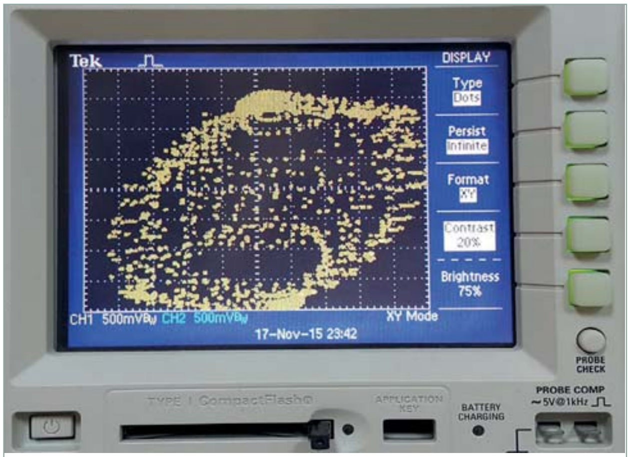

Figure 11: Real-time display for ϕ vs V1

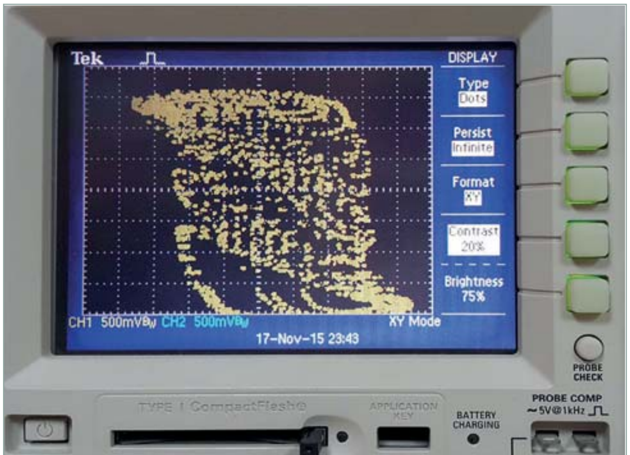

Figure 12: Real-time display for ϕ vs I

and instant values of I, V1, φ and V2 in the LabVIEW block diagram, with both obtained real and normalised attractor figures as shown in Figures 6 and 7. Two-dimensional projections of the attractors for V1-V2, V1-I, V1-φ, I-φ are shown in Figures 9-12. The oscilloscope results coincide with those of the simulation and real-time application.

Working Memristors

Memristor studies still carry on theoretically, but, in practice we don't expect to see a working, widely-available memristor for another decade, at least. It is of immense importance to build these devices, which will help secure communication systems for applications that need them. ●

AN ELECTRONIC CARD FOR EASY CIRCUIT REALISATION OF COMPLEX NONLINEAR SYSTEMS

AKIF AKGUL, FROM SAKARYA UNIVERSITY IN TURKEY, DESCRIBES THE DESIGN OF A BOARD THAT SIMPLIFIES THE DEVELOPMENT OF COMPLEX CHAOTIC CIRCUITS

The study of chaos deals with the most complicated steady-state behaviour known in dynamic systems. It also helps explain nonlinear activities in electronic systems.

Simply put, chaos is the order of disorder. Recent years have seen rapid advancements in understanding chaos and its complexity, detecting its features and differences, and observing and analysing experimental data, some of which focus on modelling chaotic circuits.

Electronic Card For Chaotic Circuits

A continuous-time chaotic system usually consists of at least three different differential equations (Equation 1). Those with more than three are called hyper-chaotic systems, and as the

Figure 1: Circuit of a sample chaotic system

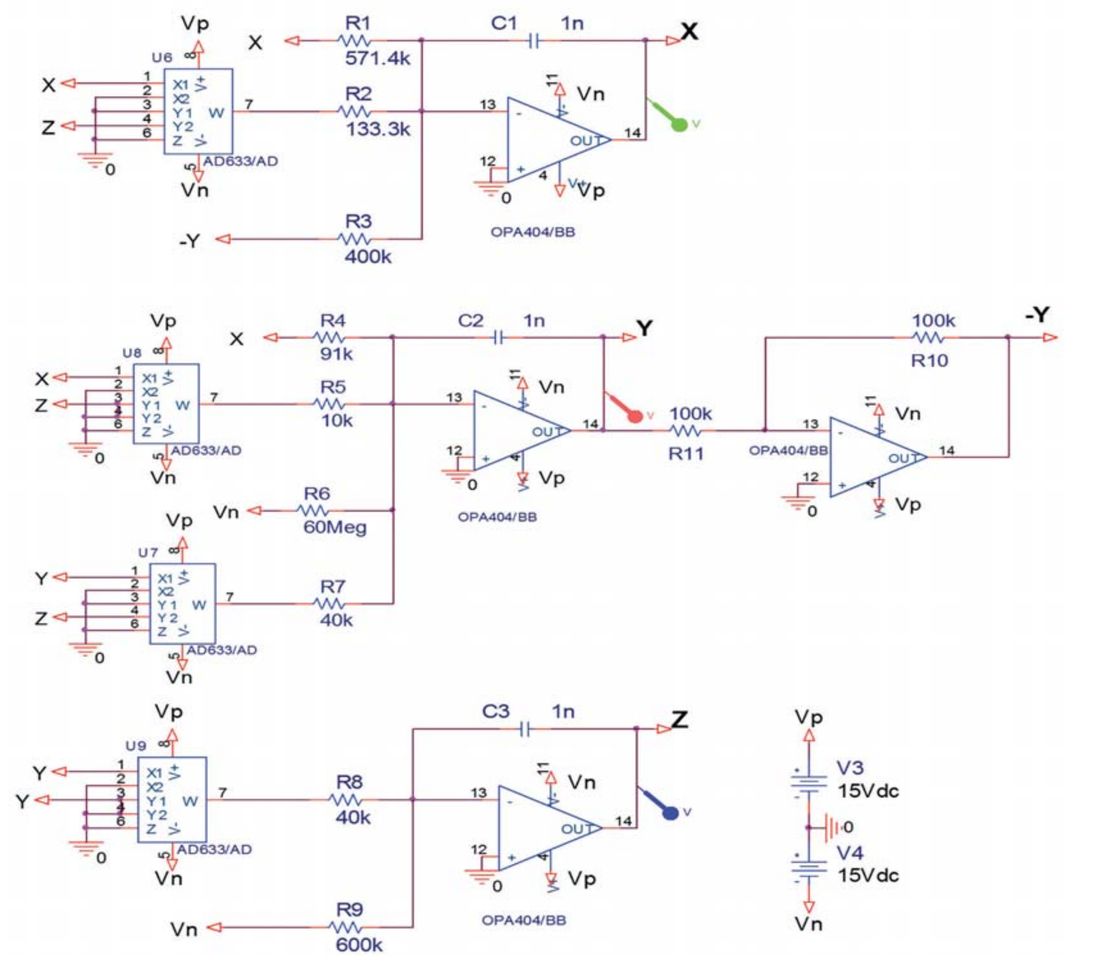

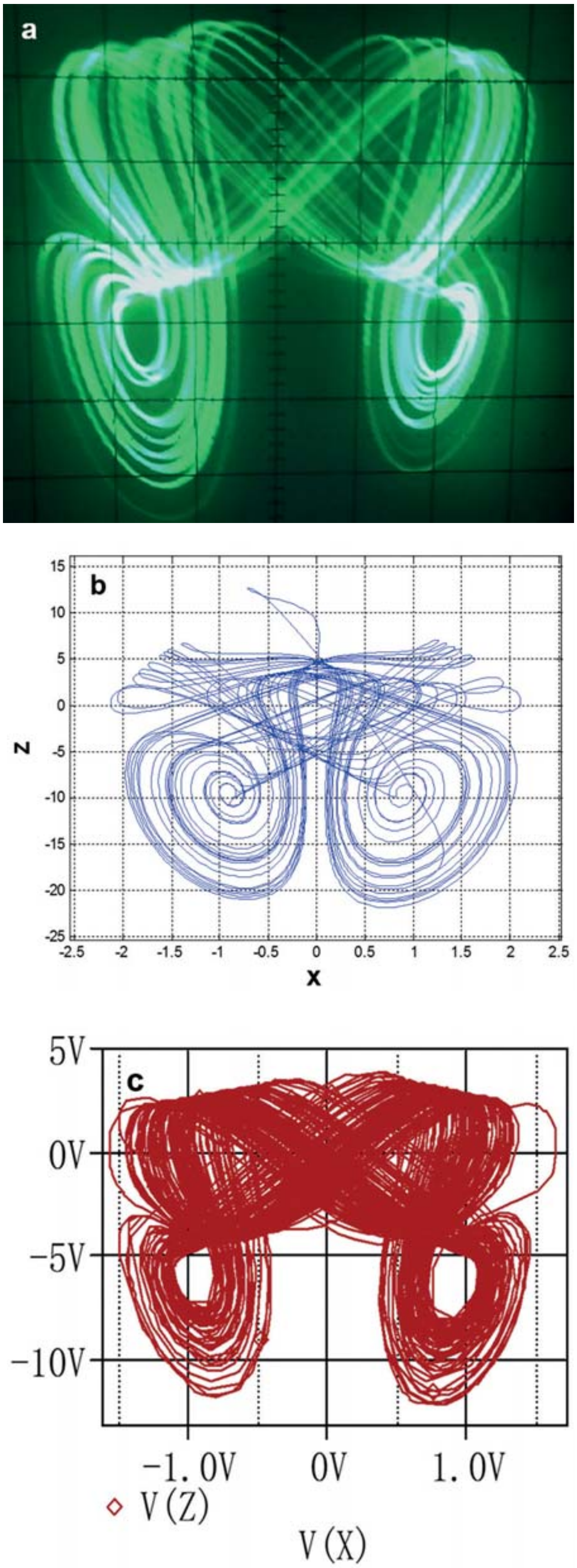

Figure 2: Oscilloscope capture in real time; (a) Matlab; (b) ORCAD-PSpice simulation programme; (c) phase outputs (x-z)

number of equations and parameters increases, it becomes harder to develop and build an electronic model of it.

$$\begin{cases} \dot{x} = y - ax + bxz \\ \dot{y} = -cxz - dx + yz + e \\ \dot{z} = f - y^2 \end{cases} \qquad (1)$$

To electronically model a chaotic system, various components are used to help determine its phase and time behaviour.

Figure 1 shows the electronic equivalent of Equation 1, containing resistors, capacitors, an analogue multiplier, an op-amp and an inverter.

Figure 2 shows an oscilloscope displaying Matlab, ORCAD-PSpice and phase outputs of the circuit in Figure 1.

Circuits modelled from chaotic systems are very complicated, and take a lot of time and effort to build. When different circuits are realised consecutively, the workload becomes even greater; to simplify it, we developed an electronic card.

The most common components in a chaotic circuit are analogue multipliers and op-amps (see Figure 1); the analogous electronic card has sections consisting of these and other components.

An analogue multiplier section is used for multiplication like xz and -xy; see Equation 1. The Analog Devices AD633 analogue multiplier is generally used in circuit building, and we also applied it to our circuit. Passive and other components can be used in the middle section (see Figure 3), whereas the third section is the op-amp part that integrates the operation and inverting processes. If a chaotic system has three equations and there is no inverting process, a minimum of three op-amps is needed for its op-amp section.

A ±15V symmetric power supply is also required to run the analogue multiplier and op-amps.

Figure 3: Breadboard for chaotic circuits

Chaotic Circuit Application

Figure 3 shows the parts of the chaos card: On the left is the analogue multiplier section; the solderless prototyping breadboard is in the centre, which can host any active or passive components; and the op-amp section is on the right.

Figures 4 shows sample oscilloscope output and chaotic circuit realised with the our card.

Comparison of the ease of fabrication between the electronic card and those realised on a standard breadboard reveals that the card makes circuit realisation – typically a complicated and difficult process – a lot more simple, easy and practical. With it, many continuous chaotic circuits with or without initial conditions can be built fast and with ease.

The card affords simplicity and reduced workload, cost and time. It can be used in many areas, including industrial and laboratory projects, scientific studies, post-graduate courses and nonlinear system experiments. ●

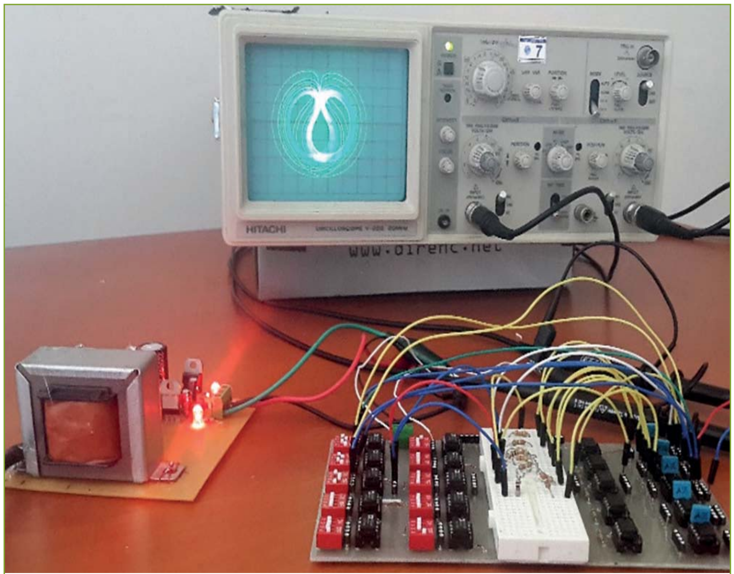

Figure 4: Sample application with the card designed for chaotic circuits

MEETING THE BOUND-VOLTAGES REQUIREMENT AND A LIGHT-SOURCE APPLICATION

MARIÁN ŠTOFKA, SLOVAK UNIVERSITY OF TECHNOLOGY, BRATISLAVA, SLOVAKIA

In electronics, occasionally there's a need to generate more than one voltage, each with a value anywhere from zero to full scale, yet with their sum a constant.

Generating a pair of complementary voltages is illustrated by the simplistic circuit shown in Figure 1, where potentiometer P divides voltage V of the source into V_x and V_y, depending on the slider position. These voltage values are:

$$V_x = R_x.I = R_x.\frac{V}{R}$$

$$V_y = R_y.I = R_y.\frac{V}{R}$$

where R_x is the resistance between potentiometer terminals B and W, and R_y the resistance between A and W; I is current:

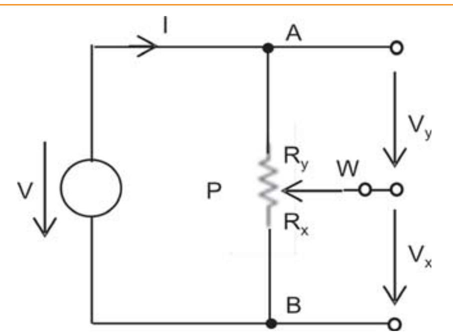

Figure 1: Simplistic way of creating two complementary voltages

$$R_x + R_y = R$$

where R is the resistance between the potentiometer's A and B terminals, a constant. Thus, R_y is:

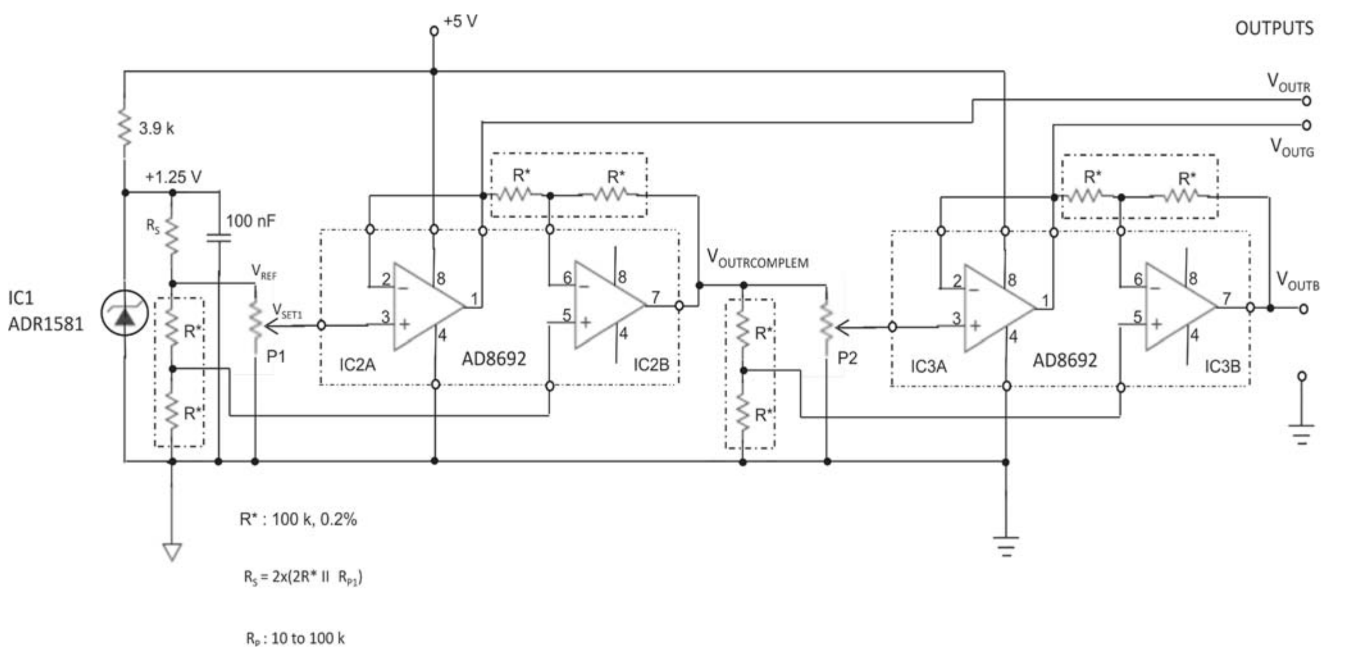

Figure 2: With potentiometers P1 and P2, a three-output voltage can be set to any level from zero to V_{REF}

Figure 3: Block diagram of a light generator with tuned colour and hue and preserved luminous flux

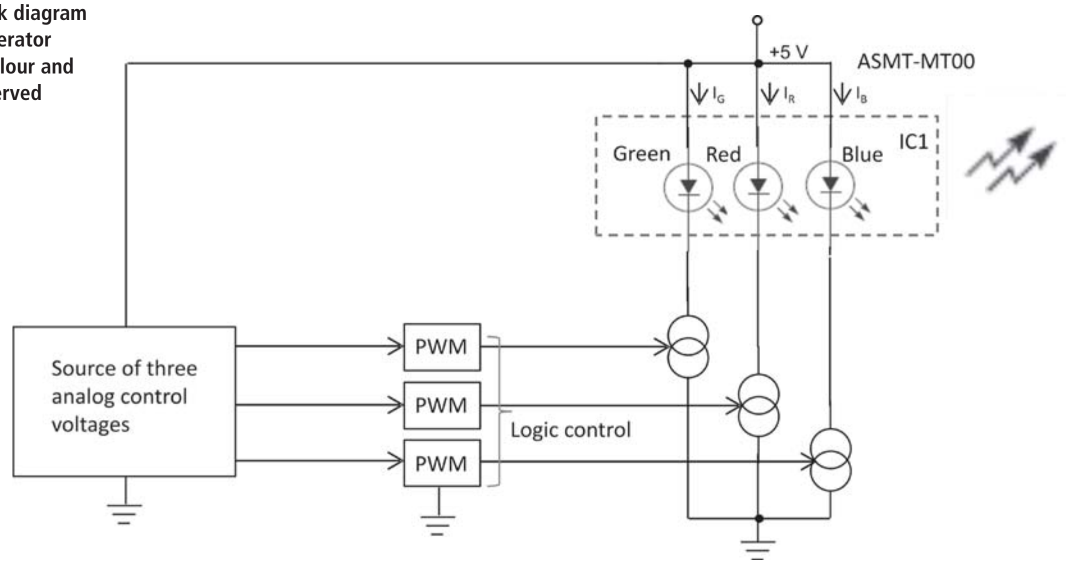

$R_y = R - R_x$

By substituting the latter into the expression for V_y, we get:

$$V_y = (R - R_x)\frac{V}{R} = V\left(1 - \frac{V_x}{V}\right)$$

from which it can be determined that V_x and V_y are complementary and their sum is a constant, V.

In practice, however, usually not only must the generated voltages be referenced to the same terminal, but they should be the same polarity, too. For this reason, the simplistic circuit in Figure 1 is not usable; if terminal B was a reference terminal or analogue ground, the voltage V_y would have to be level-shifted by $-V_x$.

Varying Voltages

The circuit shown in Figure 2 is a low-side source of three analogue voltages, with outputs V_{OUTR}, V_{OUTG} and V_{OUTB}; each can be varied from zero to full scale. Their sum is a constant (namely, full scale), given by the reference voltage V_{REF}.

When the first voltage (V_{OUTR}) is set, the remaining two (V_{OUTG} and V_{OUTB}) can be further varied from 0-100% of the complement V_{REF} - V_{OUTR}. Voltage $V_{OUTRCOMPLEM}$ is input voltage for the second stage, formed across IC3, and is complementary to V_{OUTR}. This stage is identical to that in Reference1, except of potentiometer P2, which is supplied from the complementary output of the preceding stage and not from the source of the reference voltage. Thus, the output voltages V_{OUTG} and V_{OUTB} are mutually complementary and their sum equals $V_{OUTRCOMPLEM}$:

$$V_{OUTB} + V_{OUTG} = V_{OUTRCOMPLEM} = V_{REF} - V_{OUTR} \qquad (1)$$

By rearranging Equation 1, we get:

$$V_{OUTB} + V_{OUTG} + V_{OUTR} = V_{REF} \qquad (2)$$

Thus, the sum of the three output voltages is theoretically constant, or in other words, these voltages are bound.

Circuit Operation

The accuracy of the circuit can be evaluated from the experimental results; see Table 1. The input voltage V_{SET1} has been set at full scale, mid-scale and zero, where the full-scale voltage is V_{REF} = +414.65mV.

From Table 1 it follows that the maximum relative error for zero output voltage is not greater than 3.75×10^{-3}, whereas for the mid- and full-scale it's less than 0.2%. To further clarify, if you theoretically expect, for instance, zero output voltage (0mV), whereas the measured value is 1mV, then the relative error is 1/400 = 0.25%.

All errors are of positive sign, except that of the full-output error; the errors become negative at V_{SET1} = 0mV. The occurrence of positive and negative full-output errors is still below 0.2%.

Note that high-accuracy output voltages have been achieved, although the source is low-side-referenced type. This shows the excellent properties of the Analog Devices (ADI) AD8692 op-amp. From the detailed circuit diagram, the lower supply rail (terminal) of the op-amps is connected to analogue ground.

Not all op-amps perform well when their output voltage is close to their lower supply rail. The op-amp used here, however, performs exceptionally well even under such a circumstance.

Potentiometers P_1 and P_2 in Figure 2 can be replaced by digital potentiometers, such as the AD5290, with resolution of one part in 256. ADI produces many other types, with different resolutions, digital inputs (SPI, I²C, serial, etc.) and bandwidths.

A digital potentiometer is called a "digipot". It's an IC with the three pins A, B and W identical to the terminals of a classic

Figure 4: Logic-controlled current-source

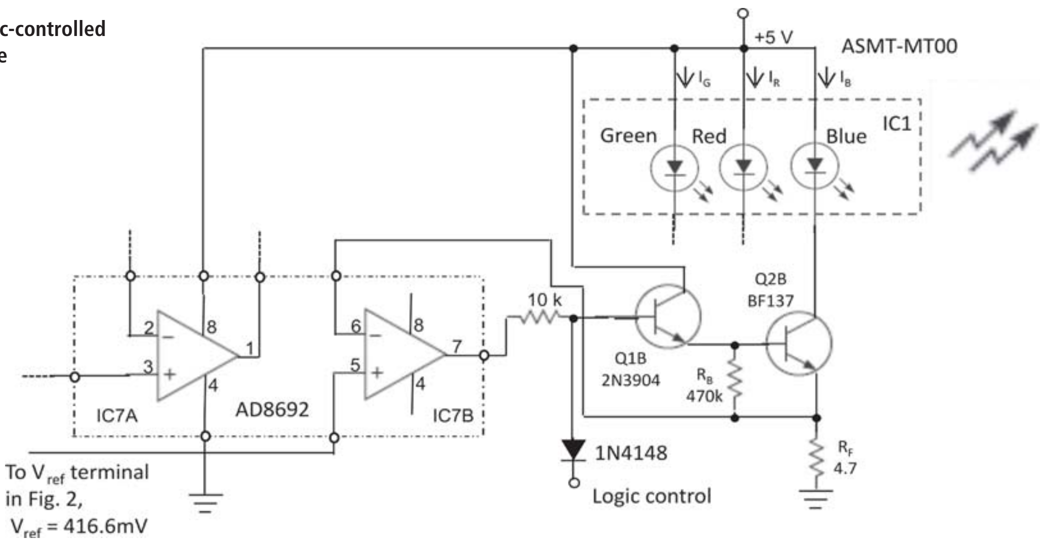

potentiometer, i.e. W is "wiper" and A and B the "ends". Resistance R_{AB} is constant, with a rounded value of, say, 20kΩ; R_{BW} is variable, set by the digital input; and R_{AW} is a complement to R_{BW}. With AD5290 in place of P_1 and P_2, the circuit in Figure 2 can be controlled by a computer.

The circuit can be used for creating any hue of light by driving red, blue and green LEDs, whilst retaining the intensity of the light output.

Circuit Application

One possible use of the circuit in Figure 2 is as a light source, producing light of desired colour and arbitrary hue, useful in many areas where colour parameters are of prime importance, such as colorimetry, for example.

The block diagram of the light source is shown in Figure 3. The actual light source is a power device, containing three LED devices, placed close to each other, commonly called "tricolour LED". The LEDs emit almost monochromatic lights – red (R), green (G) and blue (B). A mixture of their output is perceived by the human eye to be of specific colour and hue, which depends on the percentage of R, G and B.

The three blocks denoted as PWM are pulse-width modulators that convert the analogue input voltages V_R, V_G and V_B into square-wave output, with pulse widths proportional to the respective input voltages.

At the positive level of these pulses the constant-current sources I_{0R}, I_{0G} and I_{0B} turn on; during these pulses, the respective LEDs emit full-brightness light. The percentages of red, green and blue light in the final mixture depend on the width of the respective pulses at the outputs of the three PWM modulators.

The circuit shown in Figure 3 allows adjustment of red light between 0 and 100% of full scale, whereas the sum of G and B contributions represents a complement to the value of R, which is set first. The green light output can also be set between 0 and 100% of the previous complement, while the blue light percentage represents the rest of the complement that remains after setting the green light.

Driving The Circuits

The circuit shown in Figure 2 can also drive the current sources that feed the LEDs directly, but pulse-width modulators are preferable, because they drive the LEDs at a constant nominal current, eliminating any shift of wavelength in emitted light due to varying current. In addition, they also eliminate any effects of nonlinearity due to the concave luminous-flux-vs-current characteristic of the green and blue LEDs.

The luminous-flux-vs-current ratio for red, green and blue LEDs are different for a given current. For example, for the ASMT-MT00 tricolour power LED, at a given current the highest level of light flux in lumens triggers the green LED chip whereas the red LED chip triggers at roughly a third of the nominal current I_{ob}, and that of the blue LED chip at around 15%. If there is a requirement for equal flux output for all three LED chips, then the currents I_{0R}, I_{0G} and I_{0B} must be scaled:

I_{0B}: reference, or nominal current, 350mA

$$I_{0R} = 0.325 I_{0B}$$

$$I_{0G} = 0.153 I_{0B}$$

The currents are scaled by changing the value of the emitter resistor R_E of the current source to the complement of the current coefficients using bipolar transistors and op-amps (Figure 4) (see the equations above). Thus, for the ASMT-MT00 device, the values of R_{ER} and R_{EG} are:

$$R_{ER} = 3.077 R_{EB}$$

$$R_{EG} = 6.536 R_{EB}$$

R_{EB} is taken as a reference value. ●

www.electronicsworld.co.uk

December 2017/January 2018

Electronics WORLD

T&M supplement

INSIDE:

Over-The-Air Testing Of Antenna Arrays

Digital Calibration of Analogue Instruments

Ultra-High-Density Scalable Switch Matrices

from Pickering Interfaces

CONNECTING SMART HOME DEVICES TO THE WEB

> *"The word "things" in the Internet of Things are the necessary enablers, but the complete solution includes data analytics, smart phone apps and billing/support systems as well"*

Thousands of technology companies worldwide are viewing the Internet of Things (IoT) and the Smart Home as the Holy Grail for their products and profits; most industry analysts and leaders are predicting that hundreds of millions of homes will want these new technologies. However, before device makers begin to design and develop new solutions, they need to understand that this market is rapidly changing and evolving, especially when it comes to the Smart Home and the consumer electronics market.

First off, the IoT, especially for the Smart Home, is not about things, but about services that will offer consumers greater convenience and efficiency, as it will be based on better energy control and security, but also connectivity and ease of use.

Unfortunately, the word "things" in the Internet of Things tends to confuse many people, sending them on the wrong path of thinking. 'Things' are the necessary enablers, but the complete solution includes data analytics, smart phone apps and billing/support systems as well. There is an entire ecosystem at play, in which things play a (minor) role.

Also, many confuse "IoT things" with connected devices. It is not enough to just web-connect a device – it needs to be able to speak to other devices and systems in the home, as well as to be smart, i.e. utilize web intelligence for better actions, which is more than just a remotely-operated sensor or actuator.

If a manufacturer wants to be successful in the new and highly competitive IoT market, it needs to understand two important concepts:

1. The IoT and the Smart Home are not about pushing products ("things") out of the door, but about reinventing products into services. IoT business models are about recurring services and recurring revenue streams, not (only) about paying for a product at the check-out register.

2. Customers are buying solutions for problems, real or perceived. They are looking very specifically for things like security, energy control, assisted living and so on. And they want to be able to monitor and control these different solutions from one place – a single dashboard. They don't want to have to use a variety of different apps with different user interfaces (UIs) to manage their homes and their families' lives.

Manufacturers and service providers need to work together to join the different home equipment and services under a single umbrella with a common UI – a single app (say, Smart Home Butler) that allows family members to understand what goes on in their home and help them manage it, even managing it on their behalf.

The Smart Home is a wonderful concept, but as such does not solve immediate customer needs. For example, no one is looking for a refrigerator that can talk with the toaster – but if these kitchen appliances help the home shopping task simpler, if they make it easier to schedule and prepare meals, then maybe this really is an effective solution that people might be interested in. Device makers need to be very precise in what problem they are solving for their customer and evolve away from simply marketing the concept of connected devices.

The end game should be about connected solutions that make our lives easier, safer and more efficient. Device makers and service providers need to look at the "big" picture, not just the components and individual machines and devices.

Cees Links is the CEO of GreenPeak Technologies, the company that connects the devices in the Smart Home. GreenPeak Technologies is a fabless semiconductor company ***(www.greenpeak.com)***

The Family Lifestyle system uses sensors, connected devices, cloud intelligence and social media to combine a variety of important services into a simple-to-use app that enables service providers to make their customer's lives easier and more secure

Over-The-Air Testing Of Antenna Arrays

By Reiner Stuhlfauth and Dr Corbett Rowell, Technology Marketing Managers at Rohde & Schwarz in Munich

The upcoming standard for future mobile communication systems known as 5G will rely heavily on massive MIMO (multiple-input, multiple-output) systems, which combine multiple antennas with enhanced spatial multiplexing to serve multiple users.

Despite their advantages, large antenna array systems can be difficult to characterise and, in the future, it won't be possible to evaluate their radiation pattern in a conducted way, making over-the-air (OTA) connection essential.

This article presents ways to measure three-dimensional antenna patterns using OTA test setups.

5G Opportunities And Challenges

The upcoming 5G standard promises services such as enhanced mobile broadband (eMBB), ultra-reliable low-latency communications (uRLLC) and massive machine type communications (mMTC), as well as more capacity with greater flexibility – all this at lower operational expenses. To make this possible, two technologies are being discussed: virtualisation or software-defined networks (SDNs) and massive MIMO multiple antenna setups.

For wider bandwidths and consequent higher throughputs, 5G systems will use higher frequencies in the centimeter- and millimeter-wave ranges. On the flip side, however, this means higher free-space path losses. According to the well-known equation by Friis, free-space path loss depends on frequency, antenna gain and a propagation environment-specific exponent factor γ; see Equation 1.

$$\frac{P_{Rx}}{P_{Tx}} = G_{Tx}G_{Rx}\left(\frac{c}{4\pi fd}\right)^{\gamma} \qquad (1)$$

To compensate for this loss, one solution is to use antenna arrays with much higher antenna gain using beamforming (GTX and GRX). Channel analyses have shown that to maintain the same Rx power level at a frequency of 28GHz compared to 900MHz, antenna gain must increase by 30dB. This can be obtained with an antenna array with a number of antenna elements arranged for a directional characteristic, which is called beamforming. More antenna elements (usually M = 2N) results in higher gain and narrow beam width. In addition, beamforming can significantly reduce energy consumption by targeting individual user equipment (UE) with its assigned signal.

In a normal basestation without beamforming, the energy not received by the UE is absorbed into the environment or interferes with adjacent UE; see Figure 1.

The MIMO Antenna Concept

The MIMO approach is already widely used in standards like LTE or WLAN, to obtain higher capacity. This approach to spatial multiplexing exploits channel decorrelation by using multiple antennas at the channel input and output to achieve higher throughput per user. Multi-user MIMO extends MIMO by sending data to different UE simultaneously and exploiting UE's uncorrelated locations through beamforming. The phrase "massive MIMO" describes the combination of those concepts, where beamforming and spatial multiplexing combine in a dynamic way; see Figure 2.

Using massive MIMO antenna technologies offer many advantages, but it also brings challenges, too:

1. High throughput for fronthaul interface connection:

In a centralised RAN (C-RAN) architecture, the basestation connects to the centralised baseband through a fibre-optic network or microwave links. If fibre is used, it is through a digital interface, such as CPRI (Common Protocol Radio Interface), where digital I and Q (in-phase and quadrature)

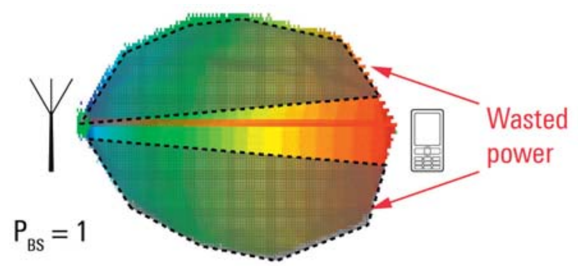

Number of BTS antenna's = 1, Number of UEs = 1	
Normalized output power of base station	1

Figure 1: Energy efficiency through beamforming

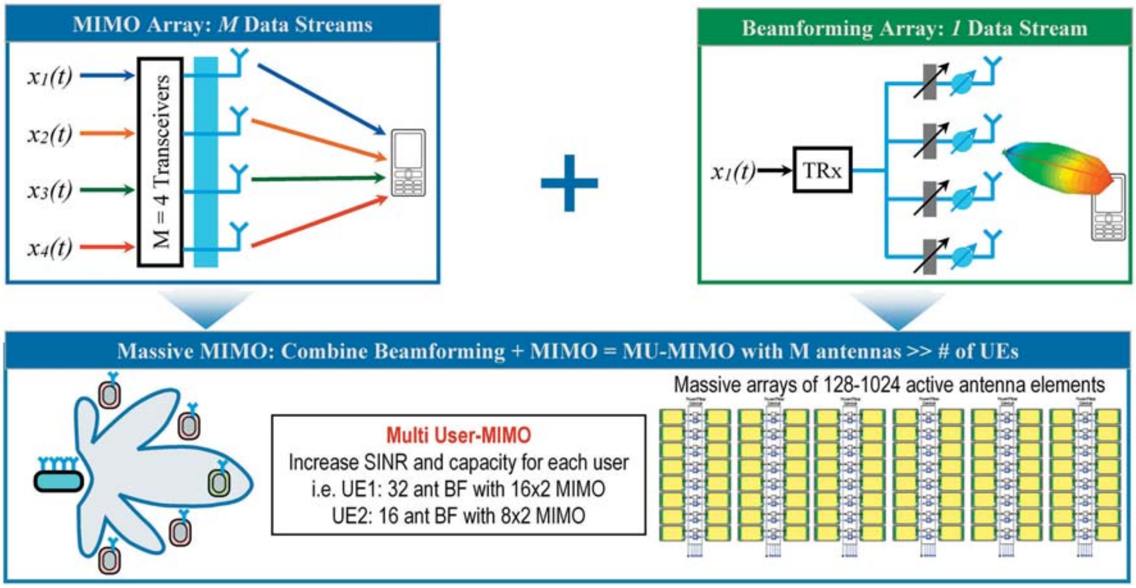

Figure 2: Massive MIMO is a combination of beamforming and spatial multiplexing

components are transmitted. The required data rate for CIPRI can be calculated as:

$$BW_{CPRI} = S \cdot A \cdot f_s \cdot b_s \cdot 2 \cdot O \cdot LC \qquad (2)$$

where S = number of sectors, A = number of antenna elements (or channels), f_s is the A/D sampling ratio, b_s is the bits/samples, O is the protocol overhead and LC is the line coding or compression scheme. As can be determined by this formula, the CIPRI bandwidth requirement scales linearly with antennas and signal bandwidth.

2. Antenna array calibration:

Due to the strict requirement of antenna array beamsteering for precise phase and amplitude differences between antenna elements, each array must be calibrated for the following tolerances:

● **Phase;**

Phase error can have a large effect on the antenna beam, depending on its statistical properties. If the phase error is uniformly distributed across the array, then the main beam direction doesn't change. Instead, the nulls that are often used to block interference are severely affected, losing 10-20dB. If there's a more deterministic phase error distribution, then this will steer the beam into a different direction, known as beam squint.

Phase error can be caused by manufacturing tolerances in the RF feeding network, thermal effects in the PAs and LNAs, and group delay variations in the filters.

● **Amplitude;**

Amplitude error does not affect beam direction, but rather the peak gain and sidelobe levels, and is generally due to thermal effects on the active components (PAs and LNAs).

● **Timing/Frequency;**

Depending on the circuit architecture, if a common LO network is not used between modules, there will be frequency drift in addition to timing errors in the ADCs.

3. Mutual coupling between antenna elements:

An antenna array is formed by placing several antennas next to each other, either in a one-dimensional line or in a two-dimensional plane.

An antenna is both a radiator and an absorber of nearby electromagnetic fields. Therefore, adjacent antennas will interact, coupling energy to other antennas, PCBs, components, etc, within the reactive near-field region of the antenna. The most common method to reduce mutual coupling is to increase the distance between antennas, but larger separations lead to bigger arrays and larger sidelobes in the antenna farfield, which increase interference for adjacent users.

Coupling effects can be measured with a Vector Network Analyser (VNA). Important to note is that transmission S-parameters between antennas allow for cross-coupling evaluation. Mutual coupling between elements of an array will decrease the radiated power level, leading to shorter cell range or smaller system capacity (reduced SNR).

The structure of the antenna array contributes directly to its mutual coupling performance. In traditional one-dimensional linear antenna arrays, each single polarised antenna element has two direct neighbours. For a uniform square array (USA) with two polarisations (co-pol and cross-pol) however, one antenna element can have up to 17 direct neighbours.

Figure 3 shows that the antenna distance between USA elements needs to become larger compared to a uniform linear array (ULA) to achieve the same channel capacity.

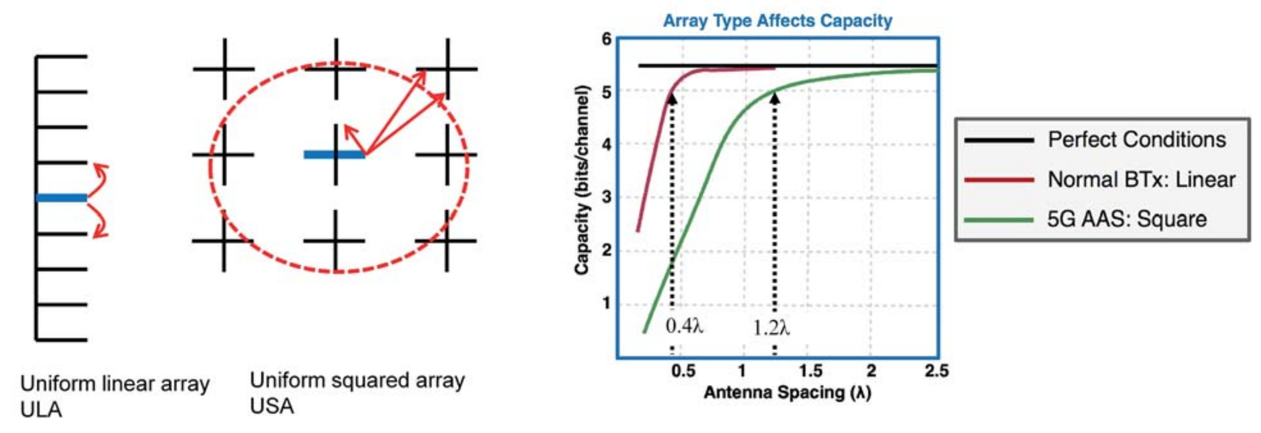

Figure 3: Mutual coupling affecting basestation capacity and range

Figure 4: Simultaneous active return loss measurement of 12 antenna elements using the R&S ZNBT20

To simultaneously measure the coupling between antenna elements in an array, a VNA with multiple ports is needed. To increase the number of connectors, a switch matrix can be connected to the DUT. This method, however, requires some switching between the measurements, which may affect performance and test duration.

True multiport VNAs are equipped with several receivers instead of switches to perform tests simultaneously, to reduce the test duration and perform a complete mutual coupling measurement between antenna element and its neighbours. If the number of antenna elements exceeds the number of simultaneous ports, switch matrices can be added.

An additional benefit is that specific tests like "active return loss" (S_{11}, S_{22}, S_{33}, ..., S_{2424}) can be measured in parallel with many ports stimulated simultaneously. This method provides deeper insights into the antenna array in the design phase, which will improve its in-situ operation in terms of network capacity.

Figure 4 shows a simultaneous, true-multiport measurement performed with the R&S ZNBT20. It shows that the active return loss is significantly different from the passive return loss, thereby requiring measuring all adjacent antenna ports simultaneously.

4. Irregular antenna arrays:

The antenna array structure ULA or USA can be replaced in practical implementations by 'invisible' antenna arrays in the shape of characters and letters, logos, or various other symbols, to blend into the background or urban environment. While these irregular arrays can reduce mutual coupling (fewer adjacent neighbours), there is of course an impact on beamforming, since the grating lobes increase and there are more side-lobes. These can be controlled by adjusting the amplitude difference between antenna elements at the cost of increased complexity.

5. Antenna array complexity:

The final challenge we discuss in this article is the drastic rise in complexity compared to current basestation antenna designs. Along the path from analogue, digital or hybrid beamforming to direct integration of radio transceivers with antennas, the number of antenna elements, RFICs, PAs, LNAs, filters, switches and duplexers rises significantly. All of which will not only determine the cost and implementation complexity but also the RF performance of the arrays.

OTA Measurements

When testing, there are two major aspects for antenna arrays that explain the necessity for OTA connection: one is the use of higher frequencies, where simple connectors can no longer be used because of increased costs, losses and coupling. Another aspect is that massive MIMO systems integrate radio transceivers directly with antennas, resulting in a loss of RF test ports. This means that DUT radio and antenna performance can only be measured with OTA interface rather than traditional

Transmitter Test	Receiver Test
Maximum Output Power	Sensitivity
EVM	Dynamic Range
ACLR	Band Selection
Spurious Emissions	Blocking (IBB, OOB, NBB)
Intermodulation	Adjacent Channel Selectivity

Table 1: A range of measurements for transmitter and receiver

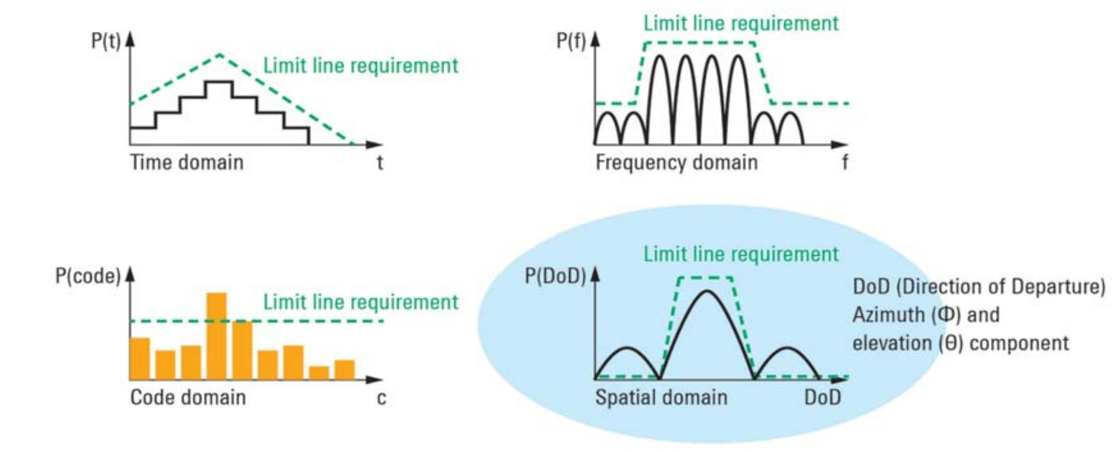

Figure 5: Power measurements as a function of time, frequency, code and space

conductive interface with a cable, which introduces a new measurement dimension – space or direction of departure.

In the past, power was measured as a function of time, spectrum, or code (CDMA systems). With beamforming another dimension is added: space or power versus direction of departure. Figure 5 shows these dimensions using an example of a power measurement.

Radiated Fields

The electromagnetic fields from any antenna can be described and measured in two different regions: near field and far field, defined by the Fraunhofer distance $R = 2*D^2/\lambda$.

In the near-field region of the antenna, at distances less than R, the field consists of both reactive and radiated components, whereas the far field has only the radiated component. For an OTA system this means that, to characterise the antenna radiation performance, the measurement can be performed in either the near-field or far-field region.

In the near-field region, a precise measurement of both phase and magnitude of the electromagnetic field over a three-dimensional surface surrounding the DUT is required for the mathematical transformation to the far-field region, resulting in antenna 2D and 3D gain patterns. A measurement in the far-field region only needs the magnitude of the field to calculate the beam pattern of the antenna, and can be measured at a single point in space, if desired.

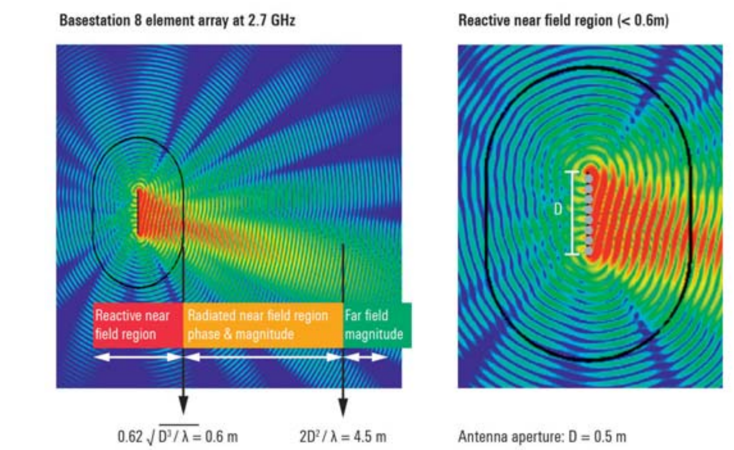

Figure 6: Electromagnetic fields from a basestation antenna array

Figure 6 illustrates the electromagnetic fields from a basestation antenna array of eight circular microstrip antenna patches at 2.7GHz with uniform excitation, where D is the maximum antenna aperture or size.

OTA measurements can be used for both absolute values like transmit radiated power, or relative values like receiver sensitivity at a specified SNR.

OTA tests measuring the three-dimensional antenna pattern can be performed either in near field or far field. Measurements in near field can be done in smaller anechoic chambers, but require instruments capable of measuring both phase and amplitude with high location precision and additional post-processing for near-field to far-field transformation.

OTA measurement parameters can be divided into two categories: R&D for more complete investigation of the DUT radiated properties and production, and calibration, verification and functional testing, summarised below.

OTA In R&D

- **Gain patterns:**

Gain patterns are either 2D from one of the three principal planes (E1, E2 or H-plane) or a complete 3D pattern, as shown in Figure 7.

- **Radiated power:**

The effective radiated power (ERP), or effective isotropic radiated power (EiRP),s is used to measure an active antenna system either as a UE or a basestation. For UE testing, total radiated power (TRP) is used instead, where TRP is the weighted integral of the ERP values over a sphere.

- **Receiver sensitivity:**

Receiver sensitivity is characterised by the parameters of effective isotropic sensitivity

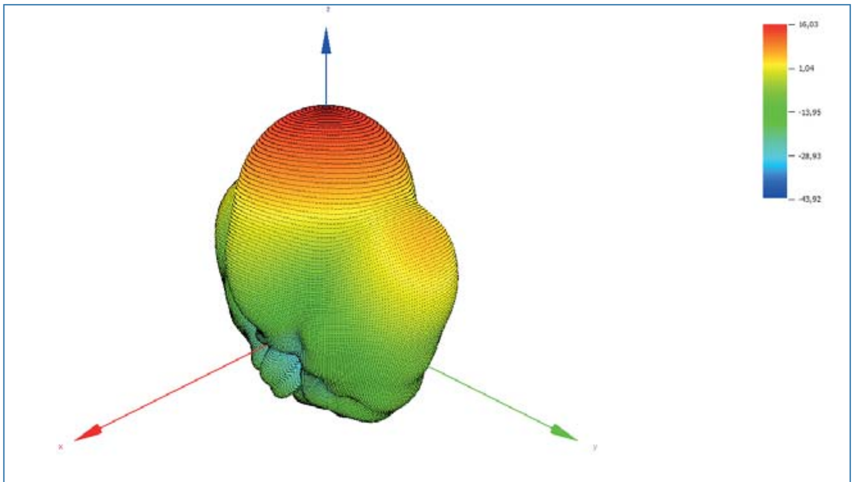

Figure 7: Example 3D antenna pattern for a small antenna array at 2.1GHz

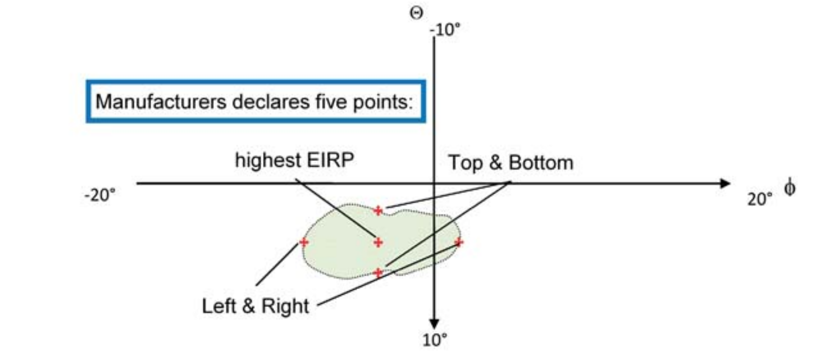

Figure 8: Five-point test based on manufacturer declaration of five measurement points

(EiS) or total isotropic sensitivity (TiS), where EiS can be calculated as TiS plus the antenna directivity. EiS effectively measures the block error rate as a function of the received power equal to the specified receiver sensitivity.

- **Transceiver and receiver characterisation:**

Each individual transceiver in the active antenna system needs to be verified through an OTA interface. This includes a range of measurements for both transmitter and receiver, as listed in Table 1. It is assumed that each transceiver will turn on for individual verification or a set of transceivers for joint assessment.

- **Beam steering and beam tracking:**

Due to the high path-loss and limited range of a mmWave wireless system, precise beam tracking and fast beam acquisition is required for mobile users. Whereas with existing cellular technologies static beam pattern characterisation was sufficient, mmWave systems will require dynamic beam measurements to accurately characterise beam tracking and beam steering algorithms.

OTA Measurements In Production Testing

- **Antenna/relative calibration:**

To accurately form beams, the phase misalignment between RF signal paths needs to be less than ±5°; greater than 5-degree misalignment typically leads to higher sidelobes, null elimination and beam misdirection. This measurement can be performed for both passive and active antenna systems using a phase-coherent receiver to measure the relative difference between antenna elements. This is then compiled into a lookup table or codebook for the active antenna system (AAS) to use as a reference for beam generation or to calibrate the internal self-calibration circuits inside the AAS.

- **Transceiver calibration:**

Due to the lack of RF ports on some massive MIMO systems, individual transceivers must also be calibrated using the OTA techniques detailed in Table 1.

- **Five-point beam test:**

According to 3GPP, the AAS manufacturer specifies beam direction, maximum EiRP and an EiRP threshold for each declared beam. In addition to the maximum EiRP point, four additional points are measured at the declared threshold boundary; see Figure 8.

- **Functional tests:**

This is the final test performed on the completely assembled unit in production. It can comprise a simple radiated test, or a five-point beam test of aggregate transceiver functionality, such as an EVM measurement of all transceivers.

OTA System Classification

OTA measurement systems can be divided into two distinct types, depending on which part of the radiated field is being sampled, as shown in Figure 6. The field regions are separated according to the power distribution of the electromagnetic field. In the reactive near-field region, the power is contained within the phase component of the electromagnetic field, whereas the radiated field in the far-field region contains power only in the magnitude of the electromagnetic wave. The region between these two extremes is the radiated near-field, where both the phase and magnitude of the field must be measured.

Most measurements are performed either in the radiated near-field or far-field region of the DUT, because any object in the reactive near-field couples to the DUT and becomes part of its effective volume.

For small devices (in terms of wavelengths), such as UE, the size is small enough so the required chamber size for far-field conditions is dominated by the measurement wavelength. For larger devices, such as basestations or massive MIMO, the required chamber size becomes very large.

Huygen's principle states that if the tangential electric and magnetic fields are known on an arbitrary surface enclosing the antenna, then the equivalent far-field radiation properties can be calculated using Fourier transforms. Chamber sizes can be reduced significantly, as long as the measurement system accurately samples the phase and magnitude of the electromagnetic field on the entire enclosing surface.

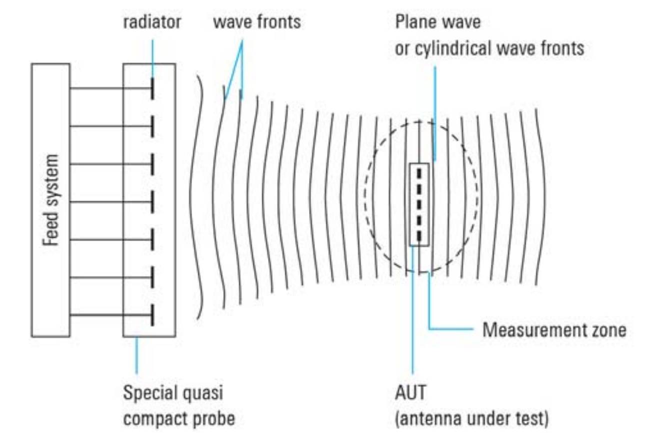

Figure 9: Plane wave conversion principle

Far-field

● **Far-field chamber size**: Measurement in the far-field region only requires a direct measurement of the magnitude of the plane waves. Such test chambers are generally quite large, where the length is set by a combination of DUT size and measurement frequencies.

● **Near-field chamber size:** Although the far field is generally measured at a suitable distance from the DUT, it is possible to manipulate the electromagnetic fields so a near-field chamber can be used to directly measure the plane wave magnitudes. There are two techniques:

i) Compact range chambers: The simplest method to form a planar wave at the surface of the DUT is to extend the path of the electromagnetic field by using reflectors, similar to optical reflectors. Due to the expense in building accurate reflectors, this technique is used mostly for large DUTs such as aircraft and satellites.

ii) Plane Wave Converter (PWC): A second method to create a planar wave at the DUT is to replace the measurement antenna with an antenna array. Like with lenses in an optics system, the antenna array can generate a planar far field at a targeted zone in the region of the DUT; see Figure 9.

Radiated near-field:

To calculate the far-field magnitude using Fourier spectral transforms, measurement in the near-field region requires both the field phase and magnitude sampled over an enclosed surface (spherical, linear or cylindrical). It is usually performed by a VNA with one port at the DUT and the other at the measurement antenna. For active antennas or massive MIMO there are often no dedicated antenna or RF ports, so the OTA measurement system must be able to retrieve the phase to complete the transformation into far field.

There are two methods of performing phase-retrieval for active antenna systems; see Figure 10:

● **Interferometric:** This method uses a second antenna of known phase as a reference. The reference signal is mixed with the DUT signal of unknown phase. Using post-processing, the phase of the DUT signal can be extracted and used for the near-field to far-field transformation.

● **Multiple surfaces or probes:** Instead of using a second antenna for phase reference, this method uses a second surface volume as the phase reference with at least one wavelength separation between the two measurement radii. As an alternative to the measurement of multiple surfaces, two probes with different antenna field characteristics can be used instead, over a single measurement surface. The two probes must be separated by at least one half-wavelength to minimise mutual coupling.

Thorough Testing Is Needed

Massive antenna arrays will play an essential role in future wireless communication thanks to many inherent advantages, but there are challenges in their development, design and production that may limit the quality expected by the end user. Thorough testing is needed to guarantee the proper working of such antenna arrays.

Due to the elimination of RF test ports and the use of frequencies in the centimeter and millimeter wave length region, OTA will become an essential tool for characterising the performance of not just the arrays of an active antenna system or a massive MIMO array, but the internal transceivers as well. For this reason, there will be high demand for OTA chambers and measurement equipment, not only to measure the radiation properties of antennas, but to make traditional transceiver measurements, too. ●

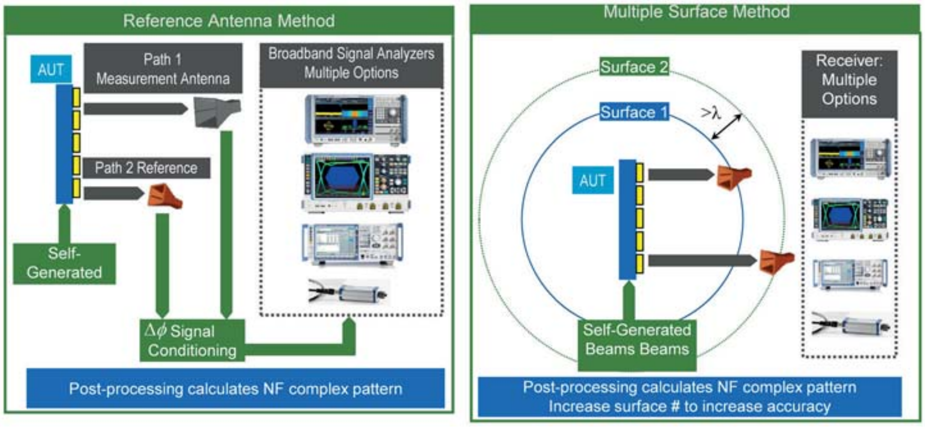

Figure 10: Radiated near-field measurement principles

Digital Calibration of Analogue Instruments

Clive Davis, European Marketing Manager for Test & Measurement at Yokogawa Europe, describes the capabilities of AC and DC voltage and current standards

In general, measuring instruments are periodically calibrated using standards to ensure the values they indicate are accurate. To take accurate yet intuitive measurements, operators expect their instruments to offer comprehensive functions, yet at smaller sizes and lower cost.

The Yokogawa models 2558A and 2560A (Figures 1 and 2) described in this article are low-cost, high-precision instruments for calibrating electric meters, thermometers, temperature transmitters and data loggers among other analogue instruments. They've been tailored to meet specific requirements for measuring equipment, discussed in detail here.

Figure 1: The Yokogawa 2558A is an AC voltage current standard that offers a high accuracy of ±0.04% for AC voltage and ±0.05% for AC current, along with a high stability of ±50ppm/h

Output-Value Digital Display

In earlier calibrator models, the output was displayed on an analogue meter, which meant the actual output value could not be read directly when measuring a deviation, or successively outputting at division points of the main set value. In contrast, the 2558A and 2560A display the value of voltage or current digitally at the output terminal. This eliminates calculating the actual output value by using the main set value, deviation and number of divisions, making calibration more efficient.

The 2558A incorporates a new mode dedicated to calibrating frequency meters. The low- and high-frequency limits of a frequency meter can be set, and this mode also provides indication of voltage and current, and functions like output sweep, step-wise output, and measurement and preset of deviation. Thus, scale accuracy, needle sticking and similar tests can easily be performed in the same way as tests of voltage or current analogue meters.

Improved Deviation Measurements

When calibrating a meter, its full scale is often different from selectable preset ranges, which can exceed the full scale of the meter. For example, if the full scale of a meter is 150V, the instrument is used with a 300V range. However, because the 2558A and 2560A allow deviation measurements with a resolution of 100ppm, this function can fully be exploited for easy calibration, without considering the meter's full scale.

When the deviation preset function is applied during a stepwise output, it is possible to gradually approach the target calibration point – either from a lower or higher value – without overshooting. This is particularly useful when the friction of the moving part needs to be accounted for. For example, two selectable preset value settings of 2% and 5% can deal with the magnitude of the torque of meter needles. This function enables convenient scale accuracy tests conforming to national and international standards.

Operating Principles

Each of the two instruments has two sections (Figure 3): the primary side that controls the oscillator output, and the secondary side, which is isolated from the primary side by transformers and a photocoupler. The oscillator signal is multiplied with the digital signal from the amplitude control section, and then amplified to provide the final output.

For voltage output, the voltage detected between the output terminals of the secondary side is converted into a digital signal and fed back to the amplitude control section via the photocoupler.

For current output, the current

Figure 2: The 2560A is the DC equivalent to the 2558A AC calibrator; it combines precision performance and ease of use for the calibration of measuring instruments including analogue meters, thermometers, temperature transmitters and data loggers

transformer detects the output current while isolating it at the same time. The detected current is converted into voltage and then into digital form at the voltage level of the primary side, to be fed to the amplitude control section. The target output level is set remotely or from the instrument panel.

In cases of substantial changes in the set value, a smoothing operation is performed to prevent overshoot or bias magnetism in the transformers caused by sharp changes in the output. After operation starts, the amplitude is adjusted every 0.4 second using the voltage or current feedback signal.

The signal fed back to the amplifier is full-wave rectified, and the ratio of the output amplitude to the set value is obtained through a level-normalisation process. A weighted average of the ratio for a certain interval is then calculated by an interval-averaging process. This average reflects the gain and similar factors of the amplifier, but is not affected directly by the set value. A gain correction coefficient is calculated from this average value to control the output amplitude.

Although not shown in Figure 3, the value used for the output indicator is a weighted interval average, calculated directly from the signal fed to the amplitude control section, without passing through the level normalisation process. Averaging and display updates occur every 0.2 seconds.

Because both the output indicator and amplitude control section use the same ADC output, when the amplitude is under stable control, the difference between the digitally-calculated target value and the displayed output value is about ±1 in the lowest digit.

Common Use Of Current Output Terminals

Whereas earlier instruments had secondary windings built into the output transformer for each current range, the 2558A output transformer includes five windings for the 10A range and none for the 50A range. The connections between these windings are switched internally for common use. For example, five windings are connected in series for the 10A range and five in parallel for the 50A range,

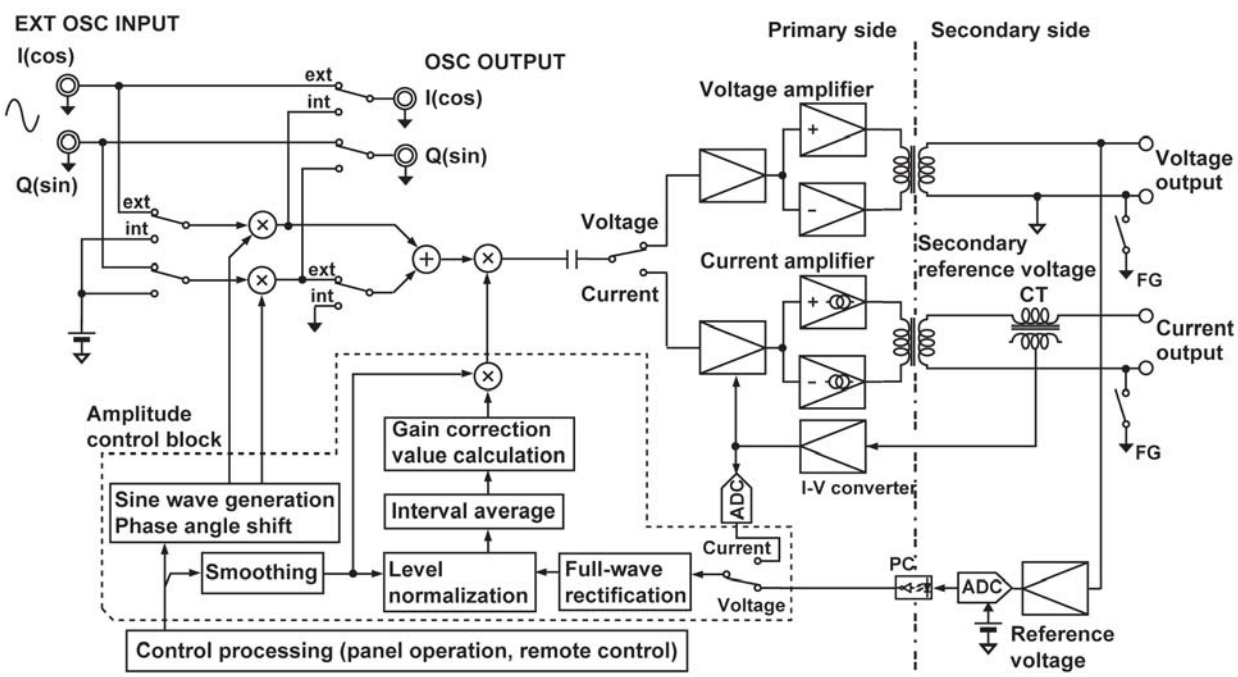

Figure 3: Block diagram of the Yokogawa 2558A

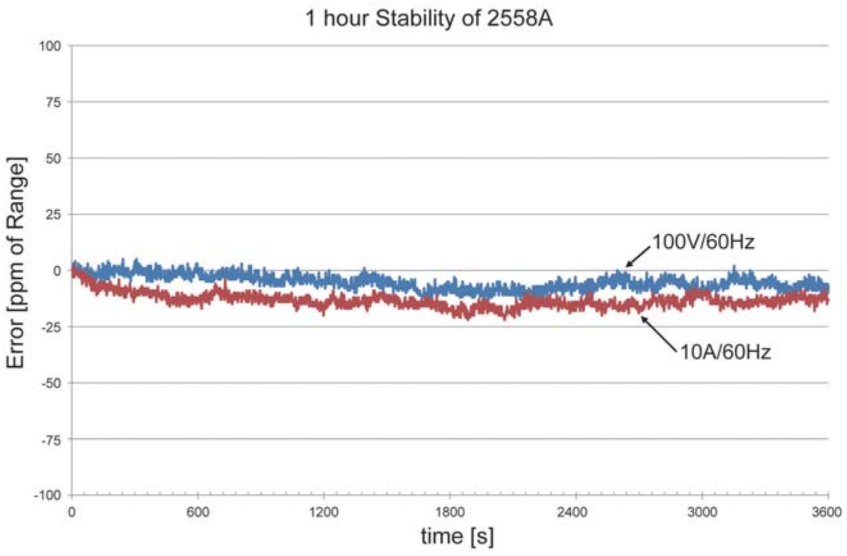

Figure 4: Measured stability of the 2558A over a one-hour period

making the transformer compact and simplifying the module's internal wiring.

Short-term stability of these units is substantially better than previous models, since they digitally process the feedback control while converting the analogue output to digital signals (Figure 4). The digital processing achieves a smooth output responding to the set value and smooth response in rising and falling waveforms, whereas earlier models sometimes exhibited overshoot or discontinuous response, depending on the load.

Dial Mechanism

In calibrating analogue instruments, operators usually manipulate the generators directly whilst watching the instrument's indicator needles. For this reason, interfaces that provide intuitive operation using setting dials and 7-segment LEDs for each digit are preferred to those using LCDs and rubber keypads.

Another requirement for these instruments is intuitive operation by dials. Because of the limited availability of rotary encoders capable of meeting this requirement, a different dial mechanism was developed. It is compact and uses miniature coil springs, spacers and other small parts, yet allows more instrument functionalities in a smaller enclosure and about 40% cheaper than previous models. These changes have also resulted in a more durable structure with continuous trouble-free operation for up to 500,000 rotations.

Applications

The 2558A allows synchronised operation of multiple units. As a result, a power calibration system can be assembled with WT3000E precision power analysers and two digital calibrators. By connecting the two instruments for synchronised operation via their rear-panel input and output terminals, the output phase of the slave can be adjusted from -180° to +360° relative to the master's output.

The phase value set on the 2558A does not guarantee the absolute phase of its output. However, this model offers very good phase stability (in practice 0.01° or less) and so it can be operated in calibration systems for watt-hour meters or other meters with the WT3000E used as a reference. The system can easily be expanded to three-phase power calibration by adding more sets.

For the direct calibration of low-frequency analogue power meters and domestic smart meters, a further development of the 2558A has been introduced – the LS3300 (Figure 5), which has a maximum frequency of 1200Hz. This instrument's key features are high phase guarantee and high power accuracy, a wide range of voltage output range up to 1250V and current output up to 62.5A, a colour LCD user interface and a choice of wiring configurations for multiphase measurements. It also allows calibration of clamp-on power meters with auxiliary outputs. ●

Figure 5: LS3300 analogue power meter calibrator

SOUTHERN MANUFACTURING & ELECTRONICS ENTERS ITS THIRD DECADE IN STYLE

Southern Manufacturing and Electronics 2018 celebrates its 20th Anniversary in style as it becomes the first major exhibition to take place in the newly-built Farnborough International Exhibition and Conference Centre, a £35m state-of-the-art permanent venue now nearing completion on the site of the iconic airshow.

The new 20,000m² Hall 1 complex, designed by award-winning architects Terence O'Rourke, is the largest exhibition venue to be built in the UK for 20 years and will completely transform the visiting experience for those travelling to Farnborough from February 6th to 8th for the UK's longest-running and biggest electronics show. Hosting an expected total of 800 participating companies, roughly half the floor area of the show will be dedicated to electronics. Encompassing production hardware and manufacturing services as well as components, Southern Electronics has carved out a well-deserved reputation as the UK's most comprehensive marketplace for electronics and related services. The size and profile of the event also makes it an attractive prospect for a steadily rising number of overseas firms – most from continental Europe but increasingly from regions such as India and the Far East as well. Many of these firms are rarely if ever seen at a UK exhibition, making a visit to Southern Electronics a unique opportunity to encounter completely new products and service providers.

For those seeking components – as around 40% of visitors annually are - the list of vendors taking part in Southern Electronics 2018 is impressive. Among the leading names taking part is Easby Electronics, one of the UK's leading independent component suppliers, carrying over 100,000 product lines. Other well-known firms taking part include Midas Components, North Devon Electronics, RJS Electronics, the Components Bureau and Nexus GB, the ruggedised memory specialists. Hylec-APL will highlight a number of new and popular products, including its UL and VDE-approved PCB terminal blocks. In addition to standard though-hole mounting and wire protected designs, there are plug and socket (right-angled and vertical), board-to-board (pluggable) and screwless, push-wire terminal blocks.

SOUTHERN
18 Electronics
FARNBOROUGH | Hants | GU14 6XL
6th to 8th February 2018

Other introductions are the TeePlug TH381 plug and socket electrical micro connector designed for underwater use and harsh environment installations and the Debox SL in-line.

The show is also a great place to source sub-assemblies and system components such as power supplies. Among the products showcased by Cosel Europe this year is the PCA series, a compact 600W AC/DC power supply offering universal main input voltage of AC6 to 264V with output voltages varying from 5.0 to 48V. The power supply is just 1U high and 152mm long and is approved for use within medical applications. It offers constant current, parallel/redundancy operation, alarm, low noise fan and remote on/off as standard. The output voltage can be adjusted close to 0V without the need for an external circuit. The latest 600W and 1200W medical grade power supplies from Delta will take centre stage on the Luso Stand. Alongside which will be products from Efore, Excelsys, N2 Power and others. Other products on show include very low power DC/DC converters, plugtops, desktop supplies, DIN rail, industrial supplies, application specific units, and fully configurable modular supplies.

Battery specialists DMS Technologies will be displaying a range of its small battery packs covering chemistries including NiMH, Li-Ion and LiFePO4. Also on the stand will be a new range of portable power products; rugged DC battery supplies for remote operating using both lithium and lead acid batteries. Alongside the UK built products will also be a range of distributed products including 12.8V Ultralife Lithium battery blocks. These offer a direct replacement to standard lead acid products, with an internal BMS meaning that they are compatible with lead acid charging systems

Among the larger manufacturers present, connector specialist ODU will be showing its new Mini-Snap self-securing circular connection, used in a multitude of applications. Whether for transferring power, signals, data or even media – this circular connector in a robust metal housing offers great long-term quality, reliability and functionality. The push-pull principle ensures connection integrity. Once mated Mini-Snap locks itself into the receptacle and can no longer be separated by just pulling on the cable. The ODU MINI-SNAP is available in a wide range of sizes and designs, and a choice of three basic keyings. Yamaichi Electronics show the recently introduced IP68-

compliant waterproof T-series expansion to its Y-Circ P circular push-pull connector family. The new waterproof T-series is based on the technology of the Y-Circ P product family, but has a new compact design. The T-series also features a one-piece collet for error-free installation and an optimised mechanism for reliable locking.

The show is also an important marketplace for engineering services such as PCB manufacture and CEM providers. One such provider is JJS Manufacturing, a long-established firm specialising in end-to-end procurement, manufacture and supply chain solutions. One of only five UK EMS companies with a wholly owned off-shore manufacturing facility JJS is a £35m turnover business delivering a wide range of assembly services including PCBA, Box Build, Cables & Wiring Looms, Cabinet Build and Electro-Mechanical assembly. There are also a good number of overseas contract manufacturers exhibiting, among them CICOR Romania, a member of the Swiss CICOR Group, an international network of electronics service providers offering a broad range of production capabilities in printed circuit board assembly, system assembly and box building, control cabinet construction, cable assembly. From even further afield, Shenzhen X-Mulong Circuit will demonstrate its range of PCB manufacturing capabilities. Established in China in 2006, the company has ISO 14001:2004 and ISO/TS 16949:2009 certification, and its products are UL and cUL-certified. The company provides PCB manufacturing services to 1,000 customers worldwide across a variety of industries, including automotive electronics, communication devices and consumer electrics.

Aside from the products and services on show, mention must also be made of the outstanding free technical seminar programme running over all three days of the show. One of the two seminar theatres is wholly dedicated to electronics sessions, covering a wide range of technical topics, including Lithium ion batteries, CE Marking, 3D Print and Industry 4.0, together with management-oriented themes such as Lean and how effectively market technical products. There is also a compelling look at the implications of the forthcoming GDPR regulations for manufacturers and the latest outlook for manufacturers post-Brexit. A full list of sessions and the all-important pre-registration form are available at http://seminars.industrysouth.co.uk

Southern Manufacturing & Electronics 2018 opens from February 6th to 8th. Admission to the show is free. More information and tickets are available from www.industrysouth.co.uk. Farnborough Exhibition and Conference Centre offers free on-site car parking and is easily reached by road, air or public transport.

CONGATEC BRINGS GERMAN INDUSTRY 4.0 EXPERTISE TO CHINA

The Taiwan located subsidiary of embedded computer modules firm Congatec is presenting smart manufacturing IT platforms for 'Made in China 2025' (MIC 2025) solutions at CIIF, China International Industry Fair (Hall 6.1H, Booth A065) in Shanghai. These platforms can be used immediately, equipping smart, connected manufacturing systems, robotics and intra-logistics devices with situational awareness for collaborative manufacturing.

The showcased Congatec MIC 2025 computer platforms feature all required interface functionalities and software support – including IIoT-based machine control and monitoring as well as maintenance clouds.

The Congatec MIC 2025 platforms are based on embedded motherboards, single board computers and Computer/Server-on-Modules, leveraging open standards freely accessible all over the world.

One of Congatec's MIC 2025 demonstrations at CIIF includes a virtualized COM Express Type 7 Computer-on-Modules based on the new Intel Atom C3000 platform (code name Denverton).

www.congatec.com

NEW AUTOMOTIVE BIPOLAR STEPPER MOTOR DRIVER IC

Allegro MicroSystems Europe introduced a new automotive bipolar stepper motor driver IC or dual DC motor driver IC, designed for pulse-width-modulated (PWM) control of low-voltage stepper motors and dual- or single high-current DC motors.

Allegro's AMT49702 is capable of output currents up to 1A per channel and operating voltages from 3.5-15V. Key applications include Heads-up-Display (HUD) – mirror positioning and dust cover, Navigation – screen lift, Driver Attention Monitor – camera movement or focus and Steering Wheel Feedback – vibration alert.

The AMT49702 is an automotive-grade device, tested across extended temperature and voltage ranges to ensure compliance in automotive or industrial applications. It has an internal fixed off-time PWM timer that sets a peak current based on the selection of a current sense resistor. An output fault flag notifies the user of a TSD or overcurrent protection event.

www.allegromicro.com

MAXIM LAUNCHES 'UNCLONABLE' SECURITY ICS

Maxim Integrated Products says that designers can now easily, proactively and inexpensively protect their products with its DS28E38 DeepCover secure authenticator chip that immunises against invasive physical attacks.

The IC features the company's ChipDNA physical unclonable function (PUF) technology, where the root cryptographic key is not in memory or any other static state but instead relies on the naturally occurring random analogue characteristics of fundamental MOSFET semiconductor devices.

When needed, the circuit generates a unique key to each device, which then disappears when not in use. If under invasive physical attack, the circuit's sensitive electrical characteristics change, further impeding the breach. In addition to the protection benefits, ChipDNA technology simplifies or eliminates the need for complicated secure IC key management as the key can be used directly for cryptographic operations.

www.maximintegrated.com

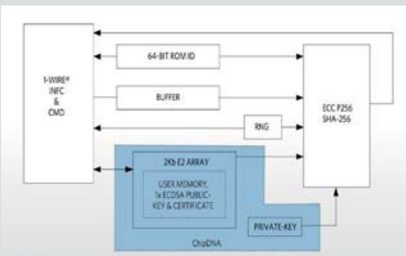

DO YOU WANT THE BEST
ELECTRONICS DESIGN SOFTWARE?
PROTEUS
The Alternatives
User Friendly
Comprehensive
Integrated
Affordable
Danger
FEATURES
• Schematic Capture
• PCB Layout
• Gridless Autorouting
• 3D Visualization
• M-CAD Integration
• SPICE Simulation
• MCU Co-simulation
• Built in IDE
• Visual Programming
labcenter
Electronics
www.labcenter.com
Tel: +44 (0)1756 753440